Selected research on woody encroachment, glacial cross-valley profiles, and mass-movement disturbance regime landscapes

by

Brandon Jeffery Weihs

B.S., University of Nebraska, 2007
M.A., University of Nebraska, 2009

AN ABSTRACT OF A DISSERTATION

submitted in partial fulfillment of the requirements for the degree

DOCTOR OF PHILOSOPHY

Department of Geography & Geospatial Sciences
College of Arts and Sciences

KANSAS STATE UNIVERSITY
Manhattan, Kansas

2020

Abstract

This dissertation is a series of stand-alone journal articles and reports produced during my tenure as a Ph.D. student. All of these articles are peer-reviewed outside the Kansas State University system, and one of them is published in *Papers in Applied Physical Geography*, a peer-reviewed journal. The following dissertation is itemized by chapters that include these pieces; Woody encroachment of a riparian corridor in a tallgrass prairie: dendrochronological evidence from Kansas, USA; Slope Failures and Cross-valley Profiles, Grand Teton National Park, Wyoming; Mass-movement Disturbance Regime Landscapes, Hazards, and Water Implications: Grand Teton National Park, Wyoming.

Selected research on woody encroachment, glacial cross-valley profiles, and mass-movement disturbance regime landscapes

by

Brandon Jeffery Weihs

B.S., University of Nebraska, 2007
M.A., University of Nebraska, 2009

A DISSERTATION

submitted in partial fulfillment of the requirements for the degree

DOCTOR OF PHILOSOPHY

Department of Geography & Geospatial Sciences
College of Arts and Sciences

KANSAS STATE UNIVERSITY
Manhattan, Kansas

2020

Approved by:

Major Professor
Douglas Goodin

Copyright

Abstract

This dissertation is a series of stand-alone journal articles and reports produced during my tenure as a Ph.D. student. All of these articles are peer-reviewed outside the Kansas State University system, and one of them is published in *Papers in Applied Physical Geography*, a peer-reviewed journal. The following dissertation is itemized by chapters that include these pieces; Woody encroachment of a riparian corridor in a tallgrass prairie: dendrochronological evidence from Kansas, USA; Slope Failures and Cross-valley Profiles, Grand Teton National Park, Wyoming; Mass-movement Disturbance Regime Landscapes, Hazards, and Water Implications: Grand Teton National Park, Wyoming.

Table of Contents

List of Figures

List of Tables

Acknowledgements

Thanks to my parents and grandparents, family, friends, coauthors, colleagues, advisers, assistants, staff, students, and neighbors. My accomplishments are possible because of the support of these people.

I thank the University of Wyoming-National Park Service Research Station, and the Association of American Geographers Mountain Geography Specialty Group Chimborazo Fund, and Mel Marcus Fund for partial funding of this project.

Dedication

This is dedicated to you, when you were young.

Chapter 1 -

Woody encroachment of a riparian corridor in a tallgrass prairie: dendrochronological evidence from Kansas, USA

Abstract

The density of forested cover in grassland regions has been increasing globally during the past several decades. While there is some evidence to suggest that climate change is playing a role in this woody encroachment, there is a lack of consensus on both the causes and consequences of this land cover change. To examine the role of climate on tree establishment and growth at a very fine spatial scale, I used dendrochronological techniques coupled with spatial analyses of the effects of climate drivers on biotic responses such as establishment and growth. I sampled ring widths of selected large trees and collected establishment dates of trees for four deciduous tree species in the riparian zone of a 119 ha experimental watershed at Konza Prairie Biological Station, near the current prairie-forest boundary of North America. Annual tree-ring width is positively correlated with the Palmer Drought Severity Index and growing season precipitation, although winter climate variables also affect deciduous tree growth. A pulse in tree establishment occurred shortly after a shift in management in the 1980s, including bison grazing and biennial burning treatments. Spatial patterns of woody vegetation expansion in this watershed indicate that recruitment is increasing at higher elevations in the riparian corridor.

Keywords: Dendrochronology, Flint Hills, PDSI, Woody Expansion, Riparian Zone

Introduction

The boundaries between grass and tree biomes have intrigued landscape ecologists for decades. Forests and grasslands have radically different ecosystem properties, such as carbon storage, albedo, and net primary productivity (Knapp et al., 2008; Barger et al., 2011). Yet, the dynamics of the boundaries including future cover have been difficult to predict. As the global phenomenon of woody expansion continues, single-factor explanations such as changes in fire (Heisler et al., 2003), grazing, land use (Archer et al., 1995), and atmospheric carbon dioxide concentrations (Bond and Midgley, 2012) have been insufficient. A more nuanced approach to spatial scale may help clarify the relative roles of climate variables in determining the dynamics of grasses and trees.

Relatively coarse (~meso-scale) climate variables such as mean annual temperature (MAT) and mean annual precipitation (MAP) explain broad patterns of forest and grass cover on both global (Staver et al., 2011) and continental scales (Sankaran et al., 2005). Sufficient precipitation (approximately 1000 mm MAP) is needed to support woody vegetation, but grassy biomes cover large areas of Earth that are mesic enough to support closed forests (Bond, 2008). In those places, disturbances such as fires and grazers are invoked to explain this apparent mismatch between climate and vegetation cover (Briggs et al., 2002; Ratnam et al., 2011).

Disturbances such as fire and grazing are important determinants of land cover at local scales (Grimm, 1984; Heisler et al., 2003). Higher disturbance frequency or severity seems to favor grassland cover and reduce forest cover. Grazing and fire together may have interactive effects that are more complicated than either factor alone (Staver et al., 2009). Disturbance can in fact shift ecosystems between alternative stable states within a single climate. For example, under moderate annual rainfall conditions (1000 to 2500 millimeters) with mild seasonality (less

than 7 months), tree cover is bimodal, and only fire differentiates between savanna and forest (Staver et al., 2011). In addition, while flood events may affect tree establishment, especially in relation to seedling uprooting, little to no flooding has occurred in this watershed in recent decades.

There is also empirical evidence for a possible role of climate at local scales of tree establishment. A dendroecological study in Minnesota, USA demonstrated that bur oak trees (*Quercus macrocarpa*) established during drought episodes, not wet times, in a savanna (Ziegler et al., 2008) and more broadly across the region (Shuman et al. 2009). Other studies such as Edmondson et al. (2014) correlated local growing season climate variables such as precipitation and soil moisture to increased ring widths of *Populus deltoides* subsp. *monilifera* in the Northern Great Plains. Spatial patterns of woody cover from aerial photographs at Konza Prairie Biological Station near the prairie-forest boundary in Kansas, USA indicate gradual expansion of woody areas since 1939 (Knight et al., 1994; Briggs et al., 2005), but potential drivers of this pattern are unclear. A better understanding of the mechanisms behind woody expansion is especially important given that tallgrass prairie is a unique and increasingly sparse ecosystem type (Samson and Knopf, 1994).

Here, I studied the history of woody cover in a single watershed in a tallgrass prairie biome through dendrochronological techniques in order to evaluate woody expansion. I sampled at both high temporal (annual) and spatial (sub-10 m scale) resolution. I had two objectives: (1) to determine the timing and spatial pattern of tree establishment in a single experimental watershed of King's Creek at Konza Prairie Biological Station, and (2) To test the relative strength of climatic drivers on facilitating tree establishment and growth, particularly exploring if the biotic response to climatic drivers varies with spatial position along the stream channel.

Methods and Materials

Study Area

This study took place along the riparian corridor (Figure 1.1) of King's Creek in an experimental watershed called N2B at Konza Prairie Biological Station (KPBS). This is a well-studied Long-Term Ecological Research (LTER) site located in the Flint Hills ecoregion, the largest continuous tract of unplowed native tallgrass prairie in North America (Samson and Knopf, 1994). Prior to its use as a research station, the area was held by private landowners who used the land for grazing cattle. In 1981, with the establishment of the LTER, the 3487-ha area was divided into sections that have been subjected to experimental treatments including the grazing of cattle and/or bison, and controlled burning at different seasons, but usually March through May. The N2B watershed is burned biennially and grazed by a herd of approximately 300 bison. Parent material in the Flint Hills is nearly-horizontal, stream-dissected, interbedded Permian limestones and shales overlain by discontinuous Quaternary alluvium (Macpherson, 1996).

Climate for the northeast region of Kansas (Kansas Climate Division Three) is characteristic of mid-continental or continental areas (Fay et al., 2011) with hot summers and cold winters. Average monthly temperatures range from -3°C in January to 27°C in July 1983-2009, with a mean annual temperature of 13°C (Craine et al., 2011). When compared with data from 1949-1979 average annual temperatures have increased 0.51°C throughout the region, with the largest increases occurring January to March (~1.67°C)(NCDC, 2012). Average annual precipitation was 927 mm (1983-2009), and ranged from 21 mm (January) to 134 mm (June). During the biologically active growing period (May-September), precipitation averaged 114 mm. Precipitation regimes have also shifted when compared to 1950-1979, with average annual

precipitation increasing 53 mm, although May to September precipitation values only increased moderately (1.25 mm) over the same period. While precipitation amounts vary considerably throughout the year regionally, drought conditions are also periodically present. A good measure of drought conditions at local scales is the Palmer Drought Severity Index (PDSI). PDSI measures deviations of monthly moisture conditions from normal conditions, indicates the intensity of long-term drought patterns, and is calculated based on precipitation, temperature, and local available water content values (Palmer, 1965).

Vegetation in the Flint Hills tallgrass prairie is dominated by C4 grasses (especially big bluestem (*Andropogon gerardii)*, Indiangrass (*Sorghastrum nutans*), switchgrass (*Panicum virgatum*), and little bluestem (*Schizachyrium scoparium*), but both hardwood (bur oak, hackberry [*Celtis occidentalis*], white ash [*Fraxinus americana*], American sycamore [*Platanus occidentalis*]) and coniferous (eastern redcedar [*Juniperus virginiana*]) trees exist, typically in or near dissected riparian corridors and lowlands. A MAP of 900 mm is mesic enough to support forest or savannah vegetation; however, historic fires, droughts, and grazing play important roles in maintaining the area as grassland (Briggs et al., 1997).

The largest stream system draining KPBS is King's Creek and its tributaries, which are medium to low in gradient (~30 to 100 m/km), dendritic in pattern, and ephemeral/intermittent, having sustained flows only in the spring season or after rainfall events, especially in headwater regions. Mean monthly discharge from King's Creek is 0.01 m^3/s in September, and 0.23 m^3/s in May (Mast and Turk, 1999). The King's Creek watershed is a Hydrologic Benchmark Network station used by the USGS as a reference watershed because it is minimally affected by human activities (Mast and Turk, 1999). Because of its reference status, King's creek was fitted with a concrete weir so that water discharge could be sampled accurately.

Riparian Corridor Tree Plots and Increment Cores

Twenty-six plots measuring 10 by 10 meters were sampled for woody vegetation along 4 km of a recently-cleared riparian corridor in the "N2B" watershed of Konza Prairie (Figure 1.1) from January to March 2011. The nomenclature for various treatments of Konza include "N" for native herbivore (bison) grazed areas, "2" for the prescribed burn regime frequency in years (1, 2, 4, or 20-year treatments), and "B" as replicate treatments (A, B, C, D). This watershed was chosen because the riparian corridor had been cleared of woody vegetation within 10 m of each side of the stream channel as part of an unrelated experiment in late fall 2010. That treatment involved cutting all woody vegetation at the ground, excepting the largest trees, which were girdled and left as standing dead trees. The remaining stumps (cut at the ground) were sanded (in situ) in order to conduct annual ring counts. Other data including trunk diameters (diameter at ground height), tree positions relative to the channel, and tree species were also documented. All stumps within each plot were sampled, resulting in a total sample size of 155 tree stumps.

The largest trees in the riparian corridor were girdled beginning in September 2010 as part of the same woody removal study. Increment cores measuring 5 mm in diameter were collected from the girdled trees (n=20) along the length of the channel. All of these trees were deciduous species: hackberry, white ash, American sycamore, and bur oak. These cores were collected following the method of Fritts and Swetnam (1989) with a Haglöf increment borer, and then were dried at 60ºC for 24 hours. Once dried, the cores were mounted into Jorgensen wood clamps, then sanded using incrementally finer grit sandpapers (up to 600 grits) until annual rings could be counted. Sanded and polished cores were then scanned using a 1200 dpi Epson flatbed scanner. These images were imported into Cybis CooRecoder 7.4 and Cybis CDendro 7.4 software for counting and measuring of rings. Heavy and negative exponent detrending (curve-

fitting algorithm) of raw ring width data was also performed in CDendro to remove age-related growth trends (Zhang et al., 2012).

Climate data from the northeast region of Kansas (1895 to 2010) was acquired from the National Climate Data Center (NCDC 2012). These data included monthly values for temperature and precipitation (minimum, maximum, mean), as well as PDSI values.

Statistical Analyses of Plot and Core Data

Stepwise multiple linear regression analysis with forward and backward elimination was used (SAS/STAT 2002) to determine which variables were predictors of mean ring width (Table 1). Variables were allowed to enter and stay in the model at the significance level of $P < 0.05$. Before the regression analyses, residuals of predictor variables were tested for normality as measured by the Anderson-Darling test (Anderson & Darling, 1954). Variables with residuals violating the assumption of normality were transformed prior to the stepwise regression. All statistical analyses were carried out in SAS 9.2. An α value of 0.05 was used to determine statistical significance.

Results

The oldest tree I sampled had established in 1880 C.E., being approximately 130 years old. The mean age of trees was 75 +/- 8 years. There were large numbers of trees established in the late 1970s to early 1980s with more than half (56%) of all plots having mean establishment dates within that range (Figure 1.2a). For individual trees within the plots, mean tree age is positively correlated with stump diameter (Figure 1.2b). There is a strong positive linear correlation between mean ages of trees in each plot and elevation of plots such that as elevation

increases, the mean tree age decreases (Figure 1.2c). This has resulted in a trend since the late 1960s of increased establishment of trees at increasingly higher elevations in the watershed, as woody species move up-channel. There was a sharp rise in both plot elevation and establishment rate around 1981, the year that Konza Prairie Long-Term Ecological Research site was established.

Annual ring widths from the 20 largest trees in the riparian corridor could be predicted by four climate variables (overall model r^2=0.311, P<0.0001) (Table 1.2). Most of the variation in ring width is predicted by the 7-year average May-June-July temperatures, with warmer temperatures leading to increased growth. Three other variables were significant at the $\alpha < 0.05$ level: August PDSI, December mean temperature, and February precipitation.

The increment cores show that a majority of the oldest trees in the riparian corridor established near the midpoint of the watershed in terms of elevation and distance to the weir (Figure 1.3). While the instrumental climate record does not extend far enough back to test if climate forcing could have caused this distribution, it is possible that moisture availability played a role in this spatial pattern. Additionally, there was a period from ~1910 to 1940 C.E. when no trees germinated, or were established in the study area.

Both climate and management variables are temporally correlated with tree establishment in the N2B watershed (Figure 1.4). Moisture availability is partially controlling tree growth and establishment, with periods of negative PDSI exhibiting lower establishment rates. An establishment pulse occurred when controlled burning practices were initiated in 1981, although the fire return interval prior to that is largely unknown. The placement of a bison herd at Konza Prairie Biological Station in 1988 with access to the N2B watershed may have slightly diminished frequency of tree establishment.

Discussion

The number of trees in the riparian corridor in the N2B watershed has been significantly increasing since the late 1800s, with the rate of tree establishment increasing since the 1970s (Figure 1.2). The fine-scale spatial pattern of this tree establishment suggests a time-transgressive pattern with trees establishing up the channel over time. Time-transgressive spatial patterns can have synchronous drivers as demonstrated by Williams et al., (2010) with regional drying and rapid-response ecotone shifts and there is evidence for synchronous drivers in this case with a strong correlation between tree growth and moist conditions as well. The strongest predictor variable for ring width was the 7-year average May-June-July temperature (Table 1.2). Other dendrochronological studies have suggested that higher growing season temperatures (May-June-July) promote tree growth in forests (Kelly et al., 2002; Garcia-Suarez et al., 2009). I found that this relationship is also supported in the more arid grassland system of Konza Prairie.

Three other climate variables affected tree growth, suggesting multiple interactions among climate and aspects of tree physiology. Increases in August PDSI were correlated to increases in ring width, which indicates that higher moisture availability during the hottest month of the year positively influences tree growth. Positive relationships between moisture and tree growth have been found in many other dendrochronological studies (Jonsson and Nilsson, 2009). However, my results differ from those at the bur oak savanna in Minnesota where drier, not wetter, times promoted tree establishment due to interactions between grass, fuel load, and fire frequency (Ziegler et al., 2008).

There are several possible explanations behind the role of winter climate variables (i.e. not during the growing season) in influencing tree growth. Increases in February precipitation were correlated to increases in ring width (Table 1.2), suggesting that precipitation in early

spring (likely snow) promotes tree growth. This indicates a potential lag effect of moisture attenuated by temperature, such that winter moisture is still important for early spring growth through infiltration and soil-water recharge. Increases in December mean temperature were also correlated to increases in ring width. While initially counterintuitive, this result points to temperature requirements for cold-hardy deciduous trees to initiate cold-hardening, bud formation, and eventual leaf formation and flowering. That is, a deciduous cold-hardy tree has several biotic responses to temperature shifts such as when cold-hardening is initiated by temperatures approaching freezing. Increases in ring width correlated to increases in December temperatures can be explained by the overarching need for a cold-hardy tree to reach temperatures capable of initiating cold-hardening but mild enough to prevent necrosis caused by extremely low temperatures affecting the ability of sugars in the cells to protect them from freezing and causing cell wall damage. Overall, these results are similar to other studies involving climate variables and tree-ring growth in that ring width is most affected by rainfall, PDSI, and maximum temperatures in the late spring and early summer (Garcia-Suarez et al., 2009), but additionally suggest that non-growing season climate variables may influence deciduous tree growth as well.

Potential reasons for a lack of establishment during the period ~1910 to 1940 include drought conditions, increased fire frequency, grazing, or human alteration (logging/clearing), although with the limited historical data available for this watershed it is difficult to evaluate these factors quantitatively. However, it is plausible that because the average PDSI index value was -0.5 for this 30-year period that tree establishment and growth could have been inhibited due to drought-induced weakening and susceptibility to stress (mildew infections, insect attacks, etc.), which can lead to mortality (Anderson et al., 2011). Moreover, this period includes the

most severe drought recorded in the U.S. (SW Kansas to N Texas), which may have killed the already stunted (by below average moisture conditions) early-stage trees established at this time.

The main spatial pattern of woody expansion for this study area is increasing establishment occurring along the riparian corridor at higher elevations and longitudinal distance from the weir. This confirms previous studies (Knight et al., 1994; Briggs et al., 2005) but also pinpoints the past few decades as an especially dynamic time. There is evidence for this woody expansion being driven by both climatic (precipitation and temperature variables) and anthropogenic factors (prescribed fire and grazing regimes set by managers). The role of additional anthropogenic factors such as increased atmospheric carbon dioxide in stimulating tree growth (Bond et al., 2012) was not addressed in this study, but could likely contribute to recruitment. Consensus as to if this conversion from tallgrass prairie to wooded grassland is reversible has not been achieved in the literature, however, several studies indicate woody encroachment decreases species richness and causes changes to community structure (Ratazjac et al., 2012). Temporal studies of this conversion in other areas suggest potential irreversibility of a shift from grass cover to tree cover (Briggs et al., 1997; Elliott, 2012). In this watershed near the current prairie-forest boundary, this may also be an irreversible shift in land cover with profound ecosystem consequences.

Conclusions

Several species of deciduous trees have expanded in spatial extent along a riparian corridor in a bison-grazed, biannually burned experimental watershed in a tallgrass prairie. These results are congruent with several other studies ranging from global to local scales, which have

documented an increase in woody cover in grassland regions (Briggs et al. 2005; Barger et al., 2011). Even in this very fine-scale study of a single riparian corridor, woody expansion was at least partially explained by climate variables such as soil moisture availability in winter months, temperature, and precipitation. There is also qualitative evidence, such as the timing of notable management events, that land use change involving grazing or burning affected the timing of tree establishment in this watershed. Future work could refine the relationships between growth, climate, and moisture sources through analyses of stable oxygen isotopes in tree-ring cellulose (Nippert et al., 2010). Another important line of inquiry would be to determine the timing and seasonal envelope of flowering, growth, and dormancy for these deciduous tree species, to better parameterize the independent climate variables that explain tree physiology and annual tree-ring growth.

It is likely that future woody expansion will continue in the N2B watershed as has been logged by this study given that the conditions that dictate this phenomenon continue, with the caveat that due to the riparian treatment (clearing the 10 m. margin of the riparian corridor), there will be seral species succession in the absence of the previous (removed) trees. This situation could prove interesting to study with fire and grazing regimes already in place at N2B, further helping to disentangle the roles of climate and disturbances on tallgrass prairie woody expansion in Kansas, and elsewhere.

Acknowledgements

I thank Jack Sparks for help conducting fieldwork, Walter Dodds for providing helpful discussion, and the Konza Prairie LTER site for initiating and conducting the woody removal experiment in N2B.

Literature Cited

Archer, S., Schimel, D.S., Holland, E.A. (1995). Mechanisms of shrubland expansion – land-use, climate or CO-2. Climatic Change Vol. 29, 91-99.

Anderson, T.W., Darling, D.A., (1954). A Test of Goodness of Fit. Journal of the American Statistical Association, Vol. 49(268), 765-769.

Andersson, M., Milberg, P.,Bergman, K.O. (2011). Low pre-death growth rates of oak (*Quercus robur* L.)-Is oak death a long-term process induced by dry years? Pages 159-168 *in* Annals of Forest Science. Springer Paris.

Barger, N.N., Archer, S.R., Campbell, J.L., Huang, C.Y., Morton, J.A., Knapp, A.K. (2011). Woody plant proliferation in North American drylands: A synthesis of impacts on ecosystem carbon balance. Journal of Geophysical Research Biogeosciences Vol. 116.

Bond, W.J., Midgley, G.F. (2012). Carbon dioxide and the uneasy interactions of trees and savannah grasses. Philosophical Transactions of the Royal Society B-Biological Sciences Vol. 367, 601-612.

Bond, W.J. (2008). What Limits Trees in C-4 Grasslands and Savannas? Annual Review of Ecology Evolution and Systematics Vol. 39, 641-659.

Briggs, J.M., Rieck, D.R., Turner, C.L., Henebry, G.M., Goodin, D.G., Nellis, M.D., (1997). Spatial and Temporal Patterns of Vegetation in the Flint Hills. Transactions of the Kansas Academy of Science Vol. 100(1/2), 10-20.

Briggs, J.M., Hoch, G.A., Johnson, L.C. (2002). Assessing the rate, mechanisms, and consequences of the conversion of tallgrass prairie to *Juniperus virginiana* forest. Ecosystems Vol. 5, 578-586.

Briggs, J., Knapp, A., Brock, B. (2002). Expansion of Woody Plants in Tallgrass Prairie: A Fifteen-Year Study of Fire and Fire-Grazing Interactions. The American Midland Naturalist, Vol. 147(2), 287-294.

Briggs, J.M., Knapp, A.K., Blair, J.M., Heisler, J.L., Hoch, G.A., Lett, M.S., McCarron, J.K. (2005). An ecosystem in transition. Causes and consequences of the conversion of mesic grassland to shrubland. Bioscience Vol. 55, 243-254.

Craine, J.M., Wolkovich, E.M., Towne, E.G., Kembel, S.W. (2011). Flowering phenology as a functional trait in a tallgrass prairie. New Phytologist Vol. 193, 673-682.

Edmondson, J., Friedman, J., Meko, D., Touchan, R., Scott, J., Edmondson, A. (2014). Dendroclimatic potential of plains cottonwood (Populus deltoides subsp. monilifera) from the Northern Great Plains, USA. Tree-Ring Research, Vol. 70(1), 21-30.

Elliott, G.P. (2012). Extrinsic regime shifts drive abrupt changes in regeneration dynamics at upper treeline in the Rocky Mountains, USA. Ecology Vol. 93, 1614-1625.

Fay, P.A., Blair, J.M., Smith, M.D., Nippert, J.B., Carlisle, J.D., Knapp, A.K. (2011). Relative effects of precipitation variability and warming on tallgrass prairie ecosystem function. Biogeosciences Vol. 8, 3053-3068.

Fritts, H.C., Swetnam, T.W. (1989). Dendroecology - a Tool for Evaluating Variations in Past and Present Forest Environments. Advances in Ecological Research 19,111-188.
Garcia-Suarez, A.M., Butler, C.J., Baillie, M.G.L., 2009. Climate signal in tree-ring chronologies in a temperate climate: A multi-species approach. Dendrochronologia Vol. 27(3), 183-198.

Grimm, E.C. (1984). Fire and other factors controlling the Big Woods vegetation. Ecological Monographs Vol. 54, 291-311.

Heisler, J.L., Briggs, J.M., Knapp, A.K. (2003). Long-term patterns of shrub expansion in a C-4-dominated grassland: Fire frequency and the dynamics of shrub cover and abundance. American Journal of Botany Vol. 90(3), 423-428.

Jonsson, K., Nilsson, C. (2009). Scots Pine (*Pinus sylvestris L.*) on Shingle Fields: A Dendrochronologic Reconstruction of Early Summer Precipitation in Mideast Sweden. Journal of Climate Vol. 22(17), 4710-4722.

Kelly, PM., Leuschner, H.H., Briffa, K.R., Harris, I.C. (2002). The climatic interpretation of pan-European signature years in oak ring-width series. Holocene Vol. 12(6), 689-694.

Knapp, A.K., Briggs, J.M., Collins, S.L., Archer, Z.R., Bret-Harte, M.S., Ewers, B.E., Peters, D.P., Young, D.R., Shaver, G.R., Pendall, E., Cleary, M.B. (2008). Shrub encroachment in North American grasslands: shifts in growth form dominance rapidly alters control of ecosystem carbon inputs. Global ChangeBiology Vol. 14, 615-623.

Knight, C.L., Briggs, J.M., Nellis, M.D. (1994). Expansion of gallery forest on Konza-Prairie-Research-Natural-Area, Kansas, USA. Landscape Ecology Vol. 9, 117-125.

Macpherson, G.L. (1996) Hydrogeology of thin limestones: The Konza Prairie Long-Term Ecological Research Site, Northeastern Kansas. Journal of Hydrology Vol. 186(1-4), 191-228

Mast, M.A., Turk, J.T. (1999). Environmental characteristics and water quality of Hydrologic Benchmark Network stations in the West-Central United States,1963–95. U.S. Geological Survey Circular (1173–C), 115 pp.

Nippert, J.B., Hooten, M.B., Sandquist, D.R., Ward, J.K. (2010). A Bayesian model for predicting local El Nino events using tree ring widths and cellulose delta O-18. Journal of Geophysical Research-Biogeosciences Vol. 115.

Palmer, W.C. (1965). Meteorologic Drought. US Weather Bureau, Research Paper No. 45.

Ratnam, J., Bond, W.J., Fensham, R.J., Hoffman, W.A., Archibald, S., Lehmann, C.E.R, Anderson, M.T., Higgins, S.I., Sankaran, M., (2011). When is a 'forest' a savanna, and why does it matter? Global Ecology and Biogeography Vol. 20, 653–660.

Samson, F., Knopf, F. (1994). Prairie Conservation in North-America. Bioscience Vol. 44(6), 418-421.

Sankaran, M., Hanan, N.P., Scholes, R.J., Ratnam, J., Augustine, D.J., Cade, B.S., Gignoux, J., Higgins, S.I., Le Roux, X., Ludwig, F., Ardo, J., Banyikwa, F., Bronn, A., Bucini, G., Caylor, K.K., Coughenour, M.B., Diouf, A., Ekaya, W., Feral, C.J., February, E.C., Frost, P.G.H., Hiernaux, P., Hrabar, H., Metzger, K.L., Prins, H.H.T., Ringrose, S., Sea, W., Tews, J., Worden, J., Zambatis, N. (2005). Determinants of woody cover in African savannas. Nature Vol. 438, 846-849.

Shuman, B., Henderson, A.K., Plank, C., Stefanova, I., Ziegler, S.S. (2009). Woodland-to- forest transition during prolonged drought in Minnesota after ca. AD 1300. Ecology Vol. 90, 2792-2807.

Staver, A.C., Archibald, S., Levin, S.A. (2011). The Global Extent and Determinants of Savanna and Forest as Alternative Biome States. Science Vol. 334, 230-232.

Staver, A.C., Bond, W.J., Stock, W.D., van Rensburg, S.J., Waldram, M.S. (2009). Browsing and fire interact to suppress tree density in an African savanna. Ecological Applications Vol. 19, 1909-1919.

Williams, J.W., Shuman, B., Bartlein, P.J., Diffenbaugh, N.S., Webb, T. (2010). Rapid, time-transgressive, and variable responses to early Holocene midcontinental drying in North America. Geology Vol. 38, 135-138.

Ziegler, S.Z., Larson, E.R., Rauchfuss, J., Elliott, G.P. (2008). Tree recruitment during dry spells at an oak savanna in Minnesota. Tree-Ring Research Vol. 64, 47-54.

Zhang, Q.B., Li, Z.S., Liu, P.X., Xiao, S.C. (2012). On the vulnerability of oasis forest to changing environmental conditions: perspectives from tree rings. Landscape Ecology Vol. 27, 343-353.

Tables and Table Captions

	Description	Units	Source
Precipitation Variables		mm	National Climatic Data Center
Mo Precip	Total monthly precipitation		
AnPrecip	Total annual precipitation		
PrcpMJJ_7yr	7 year moving average of mean precipitation for May, June, July		
Temperature Variables		°C	National Climatic Data Center
Mo Tmean	Mean monthly temperature		
AnAvTemp	Mean annual temperature		
TempMJJ_7yr	7 year moving average of mean temperature for May, June, July		
PDSI Variables		Indices	National Climatic Data Center
Mo PDSI	Mean monthly PDSI		
AnAvPDSI	Mean annual PDSI		
PDSIMJJ_7yr	7 year moving average of mean PDSI for May, June, July		

Table 1.1. Parameters used in the stepwise multiple regression to predict mean ring widths for sampled trees in the N2B watershed of Konza Prairie Biological Station.

(A) Model		n	r^2	*F* value	*P* level
Results		110	0.311	*11.96*	<.0001

(B) Parameter	Units	*B*	SE of *B*	*p* level	Partial r^2
May, June, July 7-year mean Temperature	°C	-0.124	0.031	<.0001	0.2148
August PDSI		0.018	0.007	0.0265	0.0351
December mean temperature	°C	-0.013	0.006	0.0312	0.0320
February precipitation	mm	-0.002	0.0008	0.0366	0.0291

Table 1.2. Model fit and parameter estimates for the stepwise multiple regression predicting mean ring widths for sampled trees in the N2B watershed of Konza Prairie Biological Station.

Figures and Figure Captions

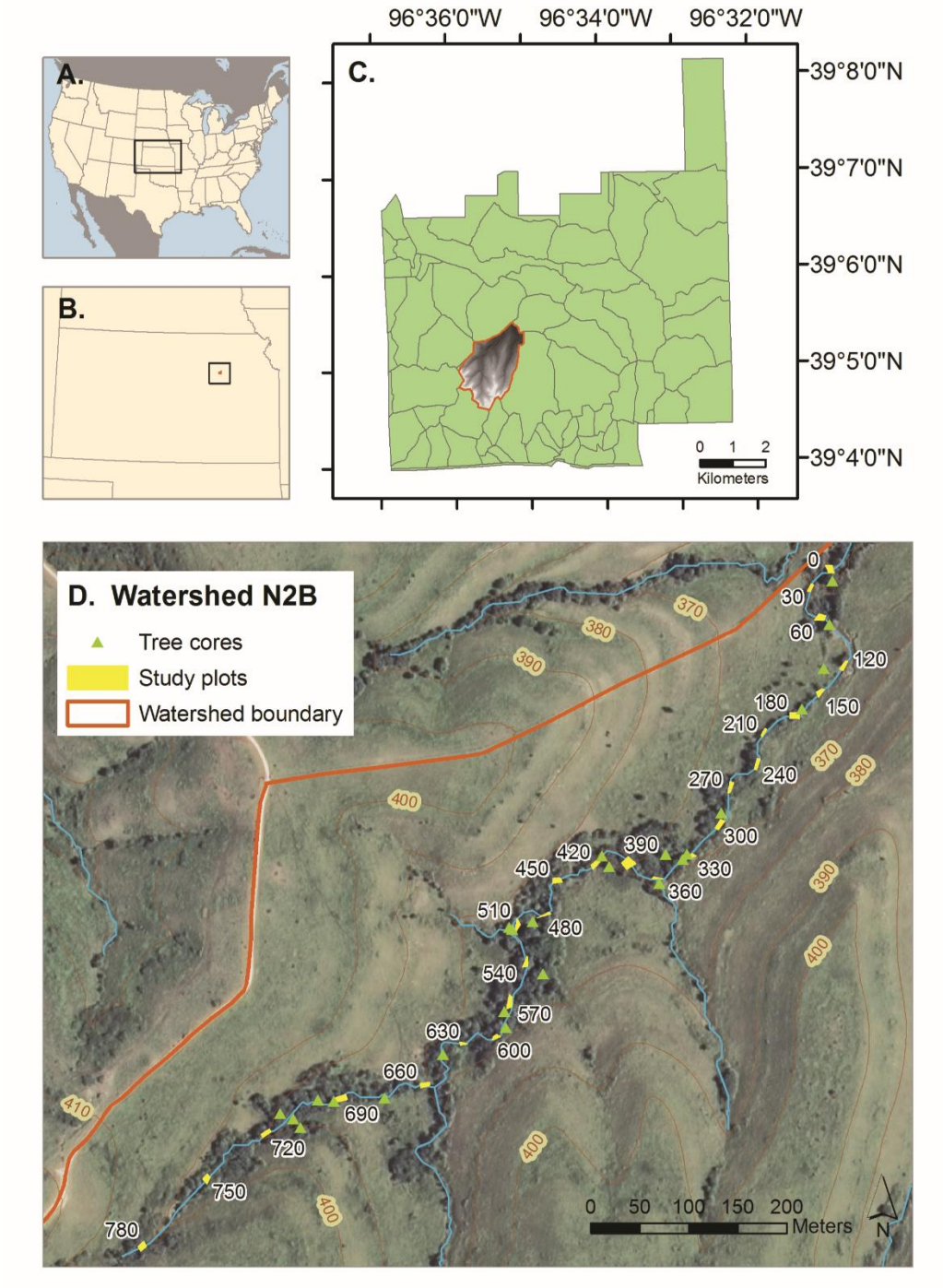

Figure 1.1 Location of study area within: (A) the United States, (B) the state of Kansas, (C) Konza Prairie Biological Station highlighting the N2B watershed, and (D) the study area within the N2B experimental watershed (weir location and plot 0 coincide).

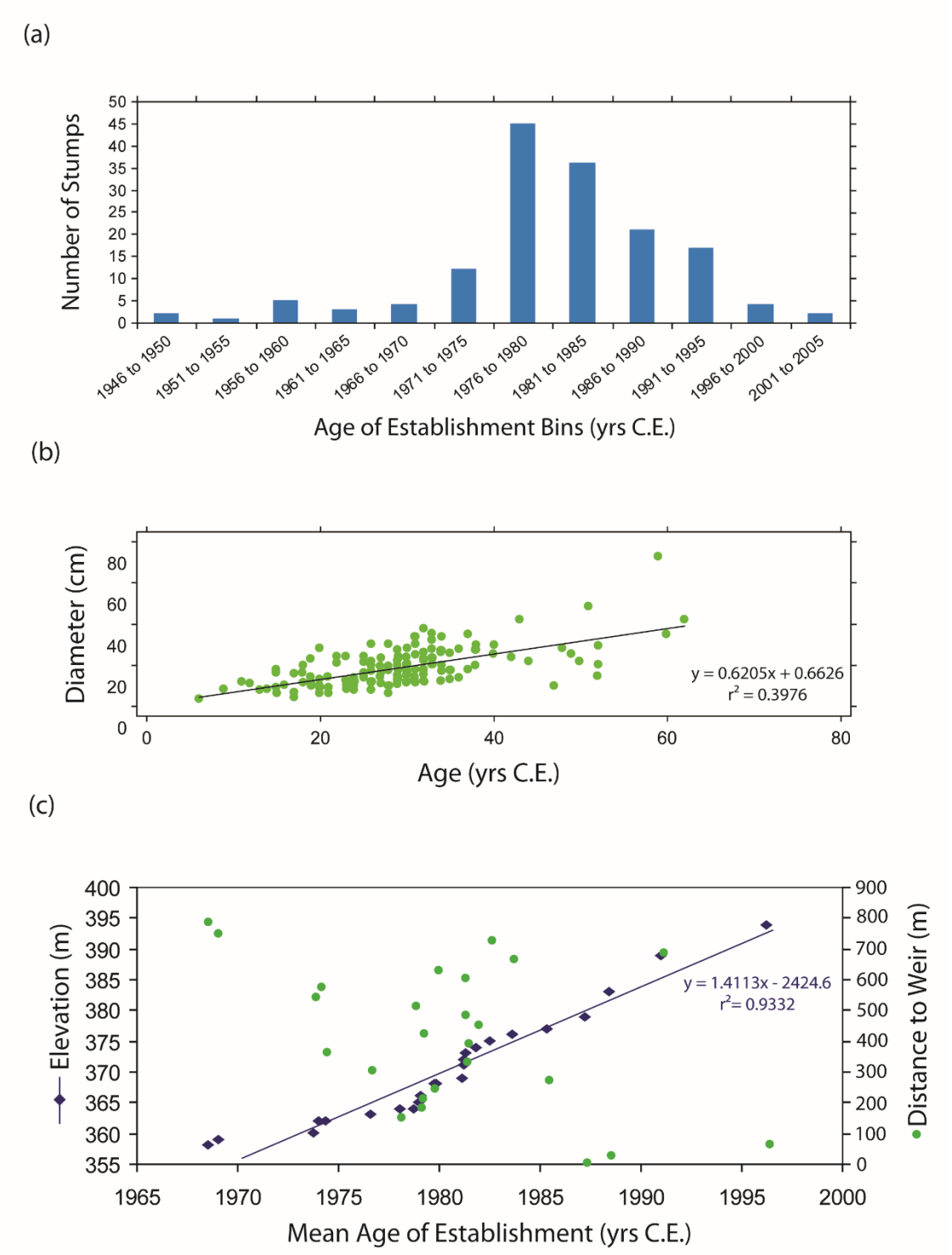

Figure 1.2. Spatial and temporal patterns of tree establishment along the King's Creek channel of the N2B watershed from the twenty-six study plots: (A) number of trees establishing in time bins during the 20th century, (B) Diameter of trees as measured from stumps < 30 cm above the soil surface, (C) mean age of establishment within a plot. Note that distance to weir for each plot can be seen in Figure 1.2C.

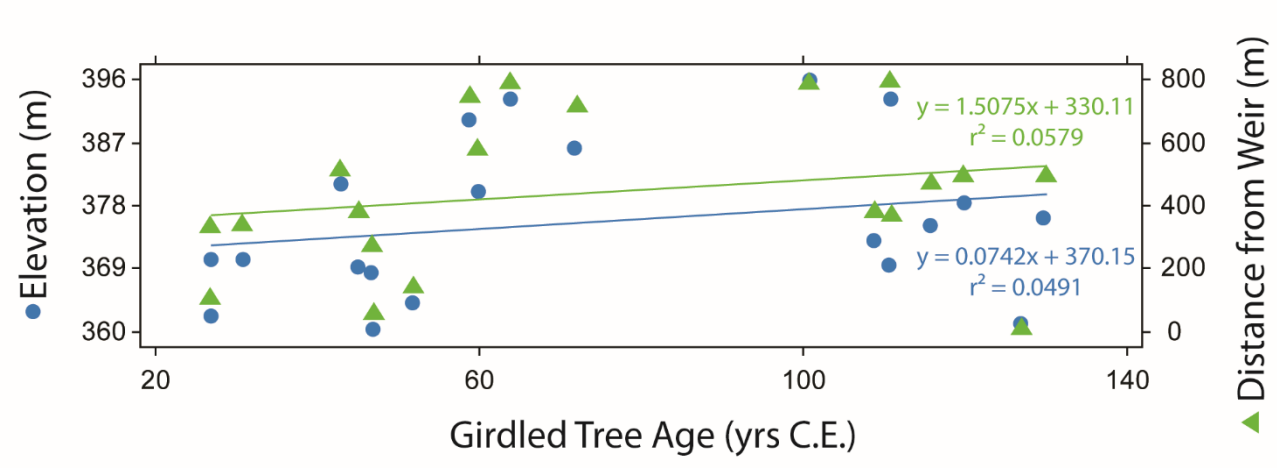

Figure 1.3. Relationship between age of the twenty largest trees in the riparian corridor, elevation, and up-channel distance.

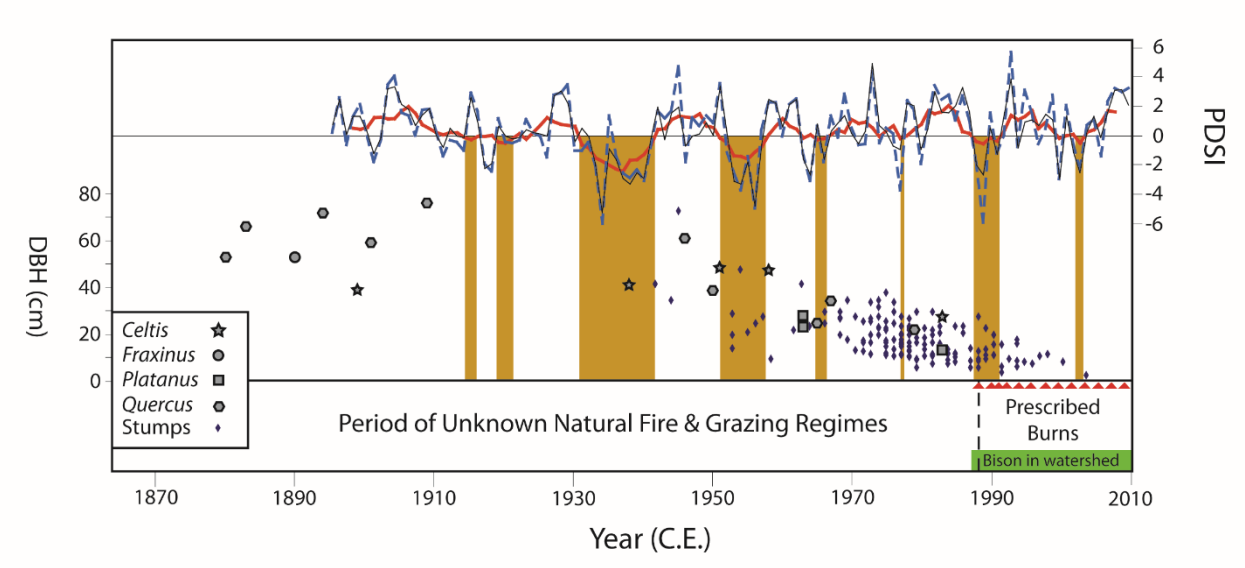

Figure 1.4. Tree diameter at breast height (dbh) for girdled trees and diameter at the base for tree stumps with approximate establishment year. The Palmer Drought Severity Index (PDSI) is calculated from the instrumental record and indicates relative moisture availability, with values below zero indicating below-average moisture availability classified as drought periods. Annual PDSI values are shown in black, May-June-July PDSI moving average values are shown in blue, and 7-year average PDSI values are shown in red. Known fires in the N2B watershed are indicated with red triangles, either prescribed or unprescribed burns. Native bison (*Bos bison*) were allowed access to the watershed in 1988, indicated with green band. Brown bands indicate significant drought events.

Chapter 2 -

Slope Failures and Cross-valley Profiles, Grand Teton National Park, Wyoming

Abstract

This project described and explained the pattern of slope failures (falls, slides, flows, snow avalanches) and the shape of valley cross-profiles in several canyons of Grand Teton National Park. Shapefiles were created in ArcMap 9.3 for slope failures using existing data sets plus newly mapped failures. Valley cross-profiles were prepared for 44 locations in the canyons using digital elevation models (DEMs). The distribution of slope failures were found to be related, to various degrees, to slope aspect, distance from the Teton Fault, rock mass strength, Schmidt rock hammer values, and slope gradient. Shape files were generated that show sections of hiking trails and camping zones that have been impacted by past events. Valley cross-profiles are best represented by a parabolic curve, and the value of the coefficient in the equation describing those curves is related to Schmidt rock hammer values and rock type. These findings have direct implications for backcountry recreation in the canyons and for visitor interpretation of canyon scenery.

Keywords: Mountain geomorphology, Deglaciated canyons, Slope failure hazard, Cross-valley profile, Rock mass strength

Introduction

Problem Statement

The shape and size of cross-valley profiles in deglaciated mountain canyons are generally recognized to be a function of rock resistance, past glacier characteristics, and time (glacier chronology and time since glaciation). Cross-valley profiles are also affected by slope failures (rock/debris falls, slides, flows, and snow avalanches), which can also pose hazards for mountain recreation. However, the patterns and controls on these phenomena are not yet well documented for Grand Teton National Park (GTNP).

Purpose and Objectives

The purpose of this project was to describe and explain the geographic patterns of glacial valley cross-profiles and slope failures in the study area canyons of GTNP, Wyoming. Specific objectives were to:

1) Map slope failures (rock/debris falls, slides, flows, and snow avalanches) and identify the key variables that control their distribution;
2) Draw valley cross-profiles, fit a mathematical curve to the data, and determine the factors that affect valley shape; and
3) Discuss the implications of 1 and 2 above to park management.

Significance

Canyons of the Grand Teton Range are used extensively by day hikers, backpackers, and rock climbers. Past slope failures have greatly modified the post-glacial canyon walls and have directly impacted trails and camping zones. This project intends to identify areas that are particularly prone to rock/debris falls, slides, flows, and snow avalanches. The canyon scenery has been shaped by past glacial episodes and subsequent slope failures (Figure 2.1).

Interpretation of the canyon scenery, through interpretative signs and guidebooks, is one goal of the National Park Service, so this project has the potential for improving the visitor experience and appreciation of the Teton landscape.

Background

Slope Failures

Mountains are affected by slope failures, classified by material involved (rocks, fine or coarse textured earth debris, or snow) along with the type and speed of movement. Slope failures comprised of either rock of unconsolidated earth debris can be classified as falls, slides, and flows. Many slope failures are complex combinations of falls, slides, and flows. A fall is a rapid type of slope failure where rocks or debris are released suddenly along a tension fracture on a cliff and the earth material falls under the direct influence of gravity. Alexander (1993) defines rock falls as mass movements that "occur through the air" from exposed rocks that are jointed and fractured on the edges of cliffs. The material commonly accumulates on a slope in the form of a talus cone (if originating from a single point on the cliff) or as a more continuous talus slope. A slide can also be composed of rocks or fine/coarse earth debris. The movement is "en mass" along a failure surface, either a plane or concave-up rotational failure surface, in which case the failure is known as a slump. Slides can range in velocity from slow to rapid. Flows vary in type because of the variety of possible materials (earth, debris, rock) and variable speeds of movement. For example, a flow can occur as a rock flow, perhaps cushioned by air as it moves rapidly downslope. These events are also known as rock avalanches (sturstroms) or blockstreams (Degenhardt et al., 2007). Other forms of flows common in mountains are debris flows (a mixture of earth material sizes) or earthflows (if earth material is fine). Flow speeds are variable and range from extremely rapid (~5 m/s) to extremely slow (~10 mm/yr) (Cruden & Varnes, 1996). The latter form is known as creep. Sidle and Ochiai (2006) note that debris slides and flows initiate on concave or linear slopes and are often started by quick rates of snowmelt, tectonic activity, and rainstorms.

Snow avalanches comprise the fourth major class of slope failures in the Teton Range. Alexander (1993) defines these movements as the result of snow packs on slopes experiencing structural instability to the point of snow movement. He also outlines the slope gradients at which snow avalanches are considered to be common and uncommon events. Small avalanches commonly occur at angles of 35 to 75 degrees, occasionally from 25 to 35 degrees, and rarely to non-existent for gradients below 25 degrees and above 75 degrees. Large avalanches commonly occur at gradients of 25 to 50 degrees, less commonly from 50 to 70 degrees, and rarely to non-existent for gradients below 25 degrees or above 70 degrees. Patten and Knight (1994) state that snow avalanches also significantly affect vegetation patterns in the park, as evidenced by their study in Cascade Canyon. One can readily identify past snow avalanche paths on aerial photography, satellite imagery, and Google Earth by locating "scars" of brush or grass on a landscape where trees have been destroyed.

Slope failures can be triggered by a number of driving forces, including:

1) Loading of slopes with weight (e.g., from water);
2) Vibrations (e.g., earthquakes);
3) Removal of lateral support (e.g., streams undercutting toes of hillslopes); and
4) Loss of strength in earth materials by increased pore water pressure (in fine textured earth materials), fissuring, solution of cementing materials, or loss of cohesion affected by plant roots.

The Teton Range is the product of high-angle block-faulting, so seismic activity will have a consistent presence at the front of the range and may trigger all four major classes of slope failures. Keefer (2002) provides a review of numerous studies that show how seismic activity can cause slope failures to occur, and Harp et al. (1981) provided the first attempt to map these seismically-induced slope failures. Therefore, treating the Teton Fault as a potential trigger of slope failures in these canyons appears to be justified.

Glacier Valley Cross-Profiles

The second objective of this study was to describe and explain the cross-profile shape of glacially eroded canyons, including the effects of slope failures. Studies concerning the geomorphological characterization of deglaciated mountain valleys have typically focused on the mathematical explanations of deglaciated valley cross-profiles, paired with the examination of hypothesized variables believed to govern profile morphology. This study, which focuses on post-glacial morphology of valley cross-profiles, is spurred by these past studies, in that past authors have made it clear that rock resistance, glacier characteristics, and time (glacier chronology and time since glaciation) must be considered together to further understand the development and form of deglaciated valleys, including post-glacial and future mass movement (Marston, 1998, 2010).

Modern textbooks incorrectly describe the cross-valley profile of deglaciated terrain as U-shaped (Christopherson, 2009; Plummer, et al., 2010; Love, et al., 2007), however connotations of the forms have been debated for approximately a century. Davis (1916) was the first to suggest that deglaciated cross-valley profiles are catenaries, which are the curves produced when a flexible, but non-stretchable chain, hangs freely from two points (Graf, 1970; Hirano & Aniya, 1988, 1989, 1990). Leibniz coined the name catenary (derived from Latin word for chain; also vernacularly called chainette) and the equation in 1691 (Smith, 1958; Lawrence, 2013). The hyperbolic cosine function (cosh) is used to define the equation for catenaries

$$Y = a \cosh (x/a), \qquad (1)$$

where x = 0 corresponds to the vertex, and *a* is the parameter that controls the width of the curve. Davis' (1916) notions about glacial valley profiles shape were followed by the work of Svensson (1959), who was the first to accurately describe deglaciated cross-valley profiles as parabolas using the power law equation

$$Y = aX^b, \qquad (2)$$

where Y is valley height, X is valley width, and *a* is a coefficient and *b* is an exponent (Graf, 1970; Hirano & Aniya, 1990). Much literature since Svensson's (1959) work has been concerned with defining the parabolic shape of deglaciated valleys using equations that have "evolved" with the addition of coefficients. An example of this "evolution" can be seen in the work of Wheeler (1984), who proposed the quadratic equation

$$Y = a + bX + cX^2, \qquad (3)$$

where Y is valley height, X is valley width, and *a*, *b* and *c* are coefficients.

Most studies characterizing deglaciated mountain valley morphology are concerned with both the shape (described by equations) of the valleys, as well as the controls of form development. Graf (1970) studied the application of fluvial concepts to glacial geomorphology, namely the effects of bifurcation ratios and the laws of stream (glacier) numbers, and stream (glacier) lengths, and Penck's law in the Beartooth Mountains of northwestern Wyoming. Harbor et al. (1988) and Harbor (1992, 1995) were concerned with mathematical modeling of deglaciated cross-valley profiles through time, and found that a key factor was the increased erosion at the thalweg of glacial channels, a result of "weaker" rocks and higher basal ice velocity in the thalwegs of glacial valleys than at the margins. Augustinus (1992, 1995) postulated that cross-profile morphology in the Southern Alps of New Zealand is a "direct consequence of the rock mass strength properties of the slope rock." (Augustinus, 1992, p.39) Hirano and Aniya (1988, 1989, 1990) investigated the differences between alpine and continental glaciations based on cross-profile morphologies (curve analyses) from other studies (including Graf 1970), and concluded that alpine glaciations are prone to overdeepening, while continental glaciations produce considerably wider subglacial valleys with different form ratios. Seppala (1978) investigated faulting and rock jointing as paramount variables in cross-valley profiles for the Lemon Creek and Ptarmigan glaciers in the Juneau Ice Field of southeastern Alaska. He found that faulting controlled the general direction of the valleys, while jointing controlled the symmetry of the cross-valley profiles.

Augustinus (1995, p.95) remarked that the need exists to develop realistic models that link glacier processes with "a scheme that incorporates feedbacks created by input of subaerial

processes…rock mass strength and stress-induced weakening of the rock mass". Harbor (1995) also noted that "future work should address more complex patterns of rock resistance to erosion, as well as non-glacial processes operating on slopes above and beyond the glacier margin" (Harbor, 1995, p.106). Brook et al. (2004) state that rock strength is an important control on glacial valley morphology. Their assertion is that rocks with higher strength values will produce steeper valley slopes, while lower strength values will produce broader valley slopes. If slope gradient is a major control on the periodicity of slope failure occurrences, then rock strength must also be considered as a critical factor. An easy, and inexpensive, way to measure rock strength is with a Schmidt rock hammer; a tool initially created/used for measuring the compressive strength of concrete. Moon and Selby (1983) played a critical role in transitioning the tool from its intended use to that of a quantitative tool used to measure Rock Mass Strength (RMS), a measure of rock stability, in the field. The technique was originally pioneered by Selby (1980) and subsequently used by Selby (1982) in the Central Namib Desert, and Moon and Selby (1983) in locations across southern Africa. RMS uses both intact rock strength measured by the Schmidt hammer and data about the joints and weathering of a rock (see Fig 2) to determine rock stability, which can be used to determine the angle at which the slope of a given landform is at equilibrium. Moon (1984) further refined the RMS technique by adding further subdivisions for intact rock strength and joint spacing. Viles et al. (2011) discuss the current debate over sampling methodology for Schmidt hammer measurements in geomorphic studies. Owen et al. (2007) studied chemical weathering rates of rock in Norway by using the Schmidt hammer, and found that periglacial (physical) erosion after the Little Ice Age overwhelmed all topographic changes caused by chemical weathering.

The combined youth of the Teton Range and the periodicity, size, and ages of glaciations make this an ideal site for studying recently deglaciated terrain and quantifying the effects of post-glacial processes on cross-valley morphology and slope failures (Pierce and Good, 1992; Love et al, 2007). Slope failures are particularly hazardous in the oversteepened mountain canyons of the Tetons, but detailed maps and statistical analyses of these forms are lacking. To understand the hazard for mass movement, it is critical to distinguish between talus, debris flows, avalanche, protalus ramparts, glacial moraines, rock glaciers and other types of coarse debris deposits such as block slides.

The hypothesis of this study was that the coefficients in the Augustinus (1992) equation will vary by rock mass strength, glacier characteristics, and time. The parabolic shape is also modified by post-glacial geomorphic processes, including by mass movement and fluvial action. The effects of these post-glacial processes on the parabolic cross-valley shape have not been modeled.

Study Area

The Teton Range is located in northwestern Wyoming at about latitude 43º 46' 46" N longitude 110º 50' 10" W (~center of range), which is approximately 10 km west of the south-flowing Snake River and approximately 5 km east of the Wyoming / Idaho state border (Figure 2.2). The range is roughly 70 km long and 20 km wide, and is the first topographic barrier to moist Pacific westerlies moving through the western Snake River Plain (Foster et al., 2010). Orographic uplift of moist air masses has contributed to glaciations in the Teton Range to cause "elevated peaks high above the surrounding topography" (Foster et al., 2010) containing isolated summits, or "topographic lightning rods" (Brozović et al., 1997; Foster et al., 2010).

The climate of GTNP at present is considered to be continental and highly variable (Vankat, 1979), having cool summers (such as near-freezing morning temperatures in July) and cold winters that are typically the lowest temperatures in the U.S., excepting parts of Alaska. According to Mahaney (1990), mean annual temperature for mountain basins is -4ºC, and mean annual minimum and maximum temperatures are -12ºC and 3ºC, respectively. Precipitation in the Rocky Mountains is also quite variable (40-150 cm), according to Vankat (1979), however, Foster et al. (2010) modeled precipitation using 30-year weather station records and found that precipitation can reach over 200 cm at the highest elevations in the range. Love et al. (2007) also note (quoting Love et al., 2003, p.95) that "modern patterns of precipitation are broadly comparable to those found in the LGM".

The flora of GTNP today is considered to be montane coniferous forest, according to Vankat (1979). This classification can be described as a mixture of altitudinal "bands" that vary with elevation, but show the same trend with changes of latitude (Vankat, 1979). In general, GTNP is dominated by coniferous trees such as *Abies lasiocarpa* (sub-alpine fir), *Abies menziesii*

(Douglas fir), and *Pinus contorta* (Lodgepole pine), but deciduous trees are also present, such as *Populus tremuloides* (Quaking aspen). In the floodplains and bottomlands, *Salix spp.* (willow) and *Artemisia spp.* (sagebrush) shrubs dominate, with various grasses and herbs existing sporadically as well. Vegetation, in the most basic of terms, decreases with altitude, and there is very little biomass above 2800 m. Vegetation of GTNP during the Pinedale glaciation would have resembled tundra conditions found only in the northernmost latitudes today. Good and Pierce (2002) described GTNP during the Pinedale as "a treeless plain", due to the incredible amount of melt-water coming out of the snout of the Jackson Lake glacier. Soils in Teton Range canyons have been described by Mahaney (1990) as poorly developed, shallow (23-68 cm), entisols (Cryorthents) and inceptisols (Cryocrepts). In general, soils are extremely young with few structures and diffuse horizonation.

Human land use is minimal in the upper reaches of most canyons in the Teton Range, having very little infrastructure excepting sporadic ranger stations, camping zones, and maintained hiking trails with timber bridges. In most respects, the Teton Range is "pristine", with virtually no direct impacts from human alteration, excepting trails, camping zones, and ranger stations that have been designed and maintained to have minimal footprints on the landscape. Beyond the mouths of the canyons though, human land use bustles, affording ski resorts, vacation homes, and GTNP to the 2.7 million (US National Park Service, 2010) annual visitors and tens of thousands of local residents. Ranching is a noticeable land use in the Snake River plain, and agriculture involving tilling is virtually non-existent. Despite the large human use of private and public lands in the area, it is flanked on nearly all sides by national forests / parks, as well as an elk refuge directly north of the city of Jackson, which limits human "interference" with natural systems to a large degree beyond the periphery of trafficable areas.

The Teton Range is the result of active crustal extension (normal faulting) and is the youngest range in the Rocky Mountains at approximately 2 million years old (Good & Peirce, 2002). This mode of orogeny sets the Tetons apart from other older (at ~80 to 55 Ma) surrounding ranges in the region, such as the Medicine Bow, Laramie, Bighorn, Beartooth, Wind River, and Absaroka Ranges (English and Johnson, 2004), which are the result of crustal shortening that produced reverse faulting (Lageson and Spearing, 1991). Uplift rates for the Teton Range are among the highest recorded in coterminous U.S., at 0.8 mm/yr (Roberts and Burbank, 1993; Foster et al., 2010). The lithology of the Teton Range is a mixture of crystalline

Archean basement rocks overlain by Paleozoic and Quaternary sediments (Love et al., 1992). The eastern flank of the range is largely free of Paleozoic rocks, due to back-tilting of the western flank (Foster et al., 2010). This back-tilting has resulted in asymmetry of the range, with high crystalline "teflon" peaks in the east, and low slopes to the west.

In terms of glaciations, the Teton Range contains evidence of at least three separate glaciations that occurred there during the Pleistocene. The Buffalo glaciation was the oldest, and likely was the result of multiple early- to mid-Pleistocene glaciations according to Mears (1974). The Bull Lake glaciation followed the Buffalo glaciation, and is roughly correlated with marine oxygen isotope (MIS) stage 6, which occurred around 190 to 130 ka (Lisiecki and Raymo, 2005). The most recent glaciation that occurred in the Teton Range was the Pinedale, which took place between 30 to 15 ka (Peirce, 2003) and is correlated with MIS 2 (Licciardi and Pierce, 2008, Pierce et al., 2018). This glaciation was considerably smaller in magnitude compared to the Buffalo and Bull Lake glaciers, and had the effect of incising smaller troughs within the larger Bull Lake troughs. This lesser amount of Pinedale ice created breaks in slope called trimlines, or "shoulders", on valley walls. Other notable features from the Pinedale glaciation exist in Jackson Hole, such as moraine dammed lakes (Jenny, Leigh, Jackson, plus others), which are a proxy for the most recent glacial extent.

Slope failures occur at extremely high rates in Teton Range. This high frequency of mass movement is largely due to tectonic and climatic forcing, coupled with the effects of variable rock types and weathering, and post-glacial debuttressing of valley walls. These colluvial processes further complicate / perturb the "misfit" fluvial regime with high and frequent debris / rock inputs which overload or even dam streams, causing epicyclical responses (Hewitt, 2006) to the constant / chaotic inputs of mass movement. This situation of continual or extended disruption of a fluvial regime has been discussed by Hewitt (2006) as a "disturbance regime", which refers to "the long-term or permanent consequences of relatively brief, but reoccurring episodes, usually of high magnitude or at critical sites", which produce landforms "whose location and history and are dependent on the disturbances" (Hewitt, 2006, p.367). According to Hewitt (2006, quoting Benda et al., 2003), the landforms of a disturbance regime "tend to be polygenetic and exhibit morphological heterogeneity", also called "patchy heterogeneous morphologies" (Burchstead et al., 2010). Though Hewitt was mostly concerned with mega-scale

rock avalanches, or sturzstrom (Shroder & Weihs, 2010), the same phases of the landslide interruption epicycle are observable in Teton canyons.

Methods

Slope Failures

To begin the process of mapping slope failures for the study canyons (Figure 2.2), the slope failure data set from the Case (1989) "Landslide map of Wyoming" (for Teton County) was imported into ArcMap 9.3 and laid over a full color orthorectified image (NAIP) of GTNP. Four primary categories of slope failures were used to group the Case (1989) data: rock falls, slides, rock/debris flows, and snow avalanches. Case's (1989) data were then further reduced to only include slope failures located within clear view of the sample sites in the study area canyons. Other data imported from the National Park Service included locations of hiking trails and camping zones.

Additional slope failures were identified and mapped in ArcMap using multiple methods: analyses of orthorectified imagery and Google Earth, spring of 2010 field reconnaissance, and photographic documentation. The full color orthorectified image provided an initial two-dimensional view of slope failure locations, while Google Earth provided a three-dimensional view to fully identify the type and shape of each deposit polygon in ArcMap. Field reconnaissance and photographic documentation provided an additional method in determining slope failure size and shape, particularly at the sample sites of each canyon. Photos were taken of both the north and south-facing slopes of the canyon to document these profiles (Figure 2.3). These photographs were used in to identify the types and shapes of slope failure polygons at each sample site.

Catchment areas (m^2) were extracted from data provided by the National Hydrology Dataset (NHD), as well as DEMs provided by the USGS. These analyses were performed using ArcHydro in ArcMap 9.3. The parameters of the catchment areas included any drainages directly

pertaining to the sample sites in each canyon and drainages within 50 meters of the beginning and end of each canyon's sample site.

Field surveying methods included rock-mass-strength (RMS) measurements taken at a sample frequency of 0.5 km along study area trunk-streams in the range (Table 2.1; red "X"s in Figure 2.4), as well as photo documentation and visual observations. RMS was quantified based on the methodology employed by Moon (1984) and described by Dackombe and Gardiner (1983), which involves the measurement of seven properties (Table 2.1). The methods used to acquire different rock properties vary; however, the end result is that each property is assigned an "r value" that is summed with the others for each sample to produce a total rating of rock mass strength. Intact rock strength sampling required the use of a Schmidt hammer (type 'R') and several measurements from a single sample location were averaged. Rock weathering and fracture continuity were qualitative assessments. Joint spacing (mm) and width of joints (m) was measured using visual observations and measurements, and GPS devices. Joint orientations were measured using a Brunton pocket transit and/or visual observations to obtain strike and dip values where possible. The outflow of groundwater from each rock sample was obtained by qualitative (visual) descriptions of water output. Compressive strength of each rock tested with the Schmidt hammer was also recorded.

Each type of slope failure in the study area canyons was mapped separately, based on the dominant processes acting on the slope and resultant deposits, to help determine the overall distribution patterns and the factors affecting the slope failures. Areas (m^2) of each deposit polygon were extracted using ArcMap, while the numbers of each type of slope failure in the canyons were also counted and analyzed statistically. Slope failure source points (the approximate initial locations of moved masses) were created in an effort to sample several variables related to slope failure where it is initiated. These points were subdivided by slope failure type (falls, flows, slides, and avalanches). Slight differences existed in source point placement methods between slope failure types. For example, debris flow deposits are often result of the convergence of several linear features (channels/ravines) which combine and produce a single deposit, whereas falls, slides and avalanches have single source cliffs, slopes, or slope facets. Flow source points were placed at positions ~1/3 of the total length of the channel from the channel/ravine heads. The remaining source points (falls, slides, and avalanches) required a single point for each deposit polygon. Fall and slide source points were placed directly

above deposit polygons, typically on the upper bounds of rock cliffs, or detachment scars, respectively. Avalanche source points were placed directly inside avalanche deposit polygons (near the tops) due to the fact that avalanche deposit delineations include both the deposits, as well as their run-out zones. This allowed source points to sample conditions causing the avalanche, not the resultant deposition area.

Once placed, slope failure source points could be used to extract several types of data in ArcMap 9.3, including; 1) Elevation (m), 2) Slope (deg), 3) Aspect (deg), 4) Distance to the Teton Fault (m), 5) Rock type, and 6) Position above/below the Pinedale Glaciation berm. These source point data were then coupled with the appropriate deposits, as well as organized by canyon/sample site locations so that RMS data could be appended to the source point data. Slope failure polygons were also analyzed in ArcMap for similar, but not identical, data types. These data include; 1) Elevation (m), 2) Aspect (deg), 3) Distance to the Teton fault (m), and 4) Relative trimline position. Once joined, these data served as the focus of further statistical analyses concerned with the presumed causes of initialization of mapped slope failures. Once compiled, the master dataset for slope failures was entered into Statistix 9.0 so that histograms could be inspected and chi-square analyses could be performed. In this manner it would be possible to identify how each environmental variable controls each type of slope failure.

This study also examined the current and potential impacts that slope failures may exert on GTNP trails and camping zones. For park trails, the total length of trails (m) intersected by an already documented slope failure polygon were counted and analyzed for each canyon using the clip function in ArcMap 9.3. Distances of trails potentially affected by slope failures within a 100 meter radius of a park trail were recorded via use of the measurement tool in ArcMap 9.3. The outermost edge of each slope failure polygon that faced the trail was used for these measurements. The length of GTNP trails intersected and/or potentially intersected by each slope failure type was also measured. Areas (m^2) of camping zones intersected by the four categories of slope failures were also recorded for each canyon using ArcMap's clip function. Potential slope failures affecting camping zones were analyzed in a qualitative table stating the slope failure type, campground name, canyon of occurrence, and whether the deposit was documented by Case (1989) or my own data collection.

Valley Cross-Profiles

Cross-valley profiles (44 total) at variable positions within study area canyons were generated using 1/3 arc second (~10 m) resolution digital elevation models (DEMs) acquired from the USGS National Map Seamless Server. These DEMs were then mosaicked using ArcMap 9.3 from ESRI (Environmental Research Systems Institute). Transect lines for cross-valley profiles were created through shapefile manipulation then exported as Excel files containing elevation data using 3-D Analyst in ArcMap 9.3. Several other datasets were created and/or used to aid in cross-profile placement and attribute entry including DEM derived surfaces (aspect, hillshade, slope, contour), orthoimagery (NAIP, DOQQs), satellite imagery (IKONOS-2) available in Google Earth™, as well as a georeferenced geology map (Love et al., 1992). Excel files containing profile elevation data were then entered into Statistix 9.0 and were used to produce quadratic equations ($y=a+bX+cX^2$) containing the coefficients needed for further analyses. These coefficients were then added to a master dataset that was used to create regressions for selected variables thought to affect valley cross-profile morphology. Other data, besides valley cross-profile coefficients, were also derived from elevation data, including longitudinal slope at cross-profiles, profile areas, Pinedale ice depth (based on trimline and valley floor elevations), form ratios (Augustinus, 1992; Graf, 1970), shear stress at valley centers, and profile distances from the Teton fault. RMS data were also appended to the new dataset and used in the subsequent analyses involving variations in valley cross-profiles.

Several output variables were combined in a master dataset which was then used to describe longitudinal variations in valley cross-profile morphology. This dataset, stratified by profiles, included variables such as profile equation coefficients, profile areas, form ratios, glacier heights, profile slopes, shear stress, rock types, and RMS variables (Table 2.2).

Form ratios were produced using the equation

$$Fr = W/D. \qquad (4)$$

where W is valley width, and D is valley depth (Graf, 1970).

Shear stress was calculated using the equation

$$T = \rho g h \sin \alpha. \qquad (5)$$

where ρ is ice density (a constant of 900 kg/m³), g is the acceleration due to gravity (9.81 m/s²), h is the thickness of the glacier, and α is the slope of the valley (Sugden & John, 1976). Values derived from this equation are expressed in terms of bars (pressure).

Profile areas were produced using the equation

$$A = (2/3)\, WD. \qquad (6)$$

where W is valley width, and D is valley depth (Dixon, 1906).

Once compiled, the master dataset for valley cross-profiles was entered into Statistix 9.0 so that summary statistics, correlation matrixes, and multi-variate regressions could be performed.

Results

Slope Failures

Locations of slope failures were mapped via shapefile creation, and an example for Cascade Canyon is shown in Figure 2.4. Inspection of histograms, and Chi-Square analyses for falls reveals that falls occur at the greatest frequency where…

1) aspect is north-facing with azimuths between 300 degrees and 60 degrees;
2) distance to the Teton Fault is between 1300 and 3700 meters;
3) Schmidt Rock hammer values are between 50-60, indicating “strong” rock; and
4) slope gradient lies in the range of 56-62 degrees.

Chi-square analyses revealed that any combination of two or more variables above produces a significant explanation (at $p < 0.0001$) for the distribution of falls.

Inspection of histograms, and Chi-Square analyses for slides reveals that slides occur at the greatest frequency where…

1) distance to the Teton Fault is between 1300 and 4100 meters; and
2) slope gradient is greater than 49 degrees.

Chi-square analyses revealed that the combination of distance to the Teton Fault and slope gradient produces a significant explanation (at $p < 0.0001$) for the distribution of slides.

Inspection of histograms, and Chi-Square analyses for flows reveals that flows occur at the greatest frequency where…

1) aspect is south-facing with azimuths between 140 degrees and 220 degrees;
2) distance to the Teton Fault is less than 3400 meters;
3) RMS is greater than 60;
4) slope gradient lies in the range of 28-54 degrees.

Chi-square analyses revealed that any combination of two or more variables above produces a significant explanation (at $p < 0.0001$) for the distribution of flows.

Inspection of histograms, and Chi-Square analyses for snow avalanches reveals that snow avalanches occur at the greatest frequency where…

1) aspect is north-facing with azimuths between 320 degrees and 40 degrees;
2) distance to the Teton Fault is between 2300 and 4800 meters; and
3) slope gradient lies in the range of 32 and 48 degrees.

Chi-square analyses revealed that any combination of two or more variables above produces a significant explanation (at $p < 0.0001$) for the distribution of snow avalanches.

The “disturbance regime” found in the Teton Range is likely the result of major climate changes that have occurred since the end of the Pleistocene. These changes, namely warming, led to the relatively recent deglaciation of the range. This removal of ice from Teton canyons, in turn, led to the debuttressing of glacially over-steepened valley walls that has apparently caused them to be unstable, likely through the redistribution of shear stresses as glacial buttressing has been removed. In general, a propensity of mass movement coincides with Pinedale trimlines in many canyons. This appears to be the result of a combination of processes such as glacial debuttressing coupled with slope aspect.

Fault-shattering and variable weathering seems to also have played a role in the frequency of mass movements in Teton canyons by weakening valley walls through continual seismic events that fracture rocks, further enabling the weathering processes to exacerbate those newly created fractures, as well as pre-existing jointing and fractures. These processes can be seen in tandem (variably) with each other throughout all sampled canyons.

Variation in slope-aspect also appears to play a large role in the type and frequency of mass movement in Teton canyons. Because many canyons more/less have east/west strikes, their valley walls are exposed to varying amounts of solar insulation, namely through northerly and southerly aspects. This is most apparent in canyons such as Cascade, Death, and Granite, where there is increased debris flow frequency on the south-facing slopes. This increase in debris flow frequency is likely due to southerly facing slopes receiving increased amounts of solar insulation, which has the effect of increasing the frequency of freeze/thaw cycles experienced on a daily basis, especially in warmer seasons. In contrast, northerly facing aspects have an increased frequency of rock falls and snow avalanches, which are likely the result of more intense frost wedging than would occur on warmer (southerly) aspects.

For the length of trails I surveyed in the field, slope failures covered the following percentages of the trail (Figure 2.5):

1) Granite Canyon 24%
2) Death Canyon 29%
3) Garnet Canyon 52%
4) Cascade Canyon 31%
5) Paintbrush Canyon 18%

For the camping zones that I surveyed, the following have been impacted by past slope failures (Figure 2.6):

1) Death Canyon Campground
2) Meadows Campground, Garnet Canyon
3) Platforms Campground, Garnet Canyon
4) Garnet Caves Campground, Garnet Canyon
5) Granite/Mt. Hunt Campground, Granite Canyon
6) Granite-Lower, Granite Canyon
7) Granite Middle/S. Fork, Granite Canyon.

Valley Cross-Profiles

An example of the valley cross-profiles is presented in Figure 2.7. The quadratic equation was fit through the points that had been derived from the DEM data. Table 2.2 contains descriptive statistics of these variables. From Table 2.2, it can be seen that all sampled rocks exhibited moderate to strong RMS ratings (53 to 78) according to the classification used by Moon (1984) (Table 2.1). Rock mass strength (RMS) seems to be at least partially responsible for the quasi-uniform cross-valley profiles of study site canyons. Because the range of RMS values for all sample sites fell within the "moderately strong" classification by Moon (1984), the parabolic shapes of cross-valley profiles are maintained as weathering and erosion compete to remove them, despite the somewhat varied lithology within individual canyons.

Shear stress in the study canyons averaged 1.6 bars, which is comparable to values from the late Pleistocene Yellowstone outlet glacier's 0.8 to 1.2 bars as reported by Pierce (2003). Given that there are several outliers over 6 bars, this average is slightly skewed as shown from Figure 2.8. These values are not outside the range of past measurements in the region. According to Peirce (2003), Locke (written comm., 2002) calculated shear stress to be as high as 8 bars in the Wind River Range icecap. A potential reason for such high shear stress was reported by Locke (2002) to be funneling of ice into steep and narrow canyons, which can partly explain the high values (6.9 bars) for two profiles in this study (D3 & D4), which are steep (0.27 & 0.31) as well as narrowing in the down-valley direction. Other canyons, such as Paintbrush,

also have steep gradients (0.24 to 0.32), which increased the inflation of the shear stress average for this study (Figure 2.9).

In an effort to understand which variables were correlated most to the C coefficients of valley cross-profiles, a correlation (Pearson) matrix was created. This matrix provided both r and p (correlation and probability) values for all dependent and independent variables from the master dataset. Based on the results of the correlation matrix, variables which had the highest r and p values (concerning the C coefficient) were used in a stepwise linear regression analysis in Statistix 9.0. This regression included C coefficients, rock type, hammer values, and joint widths, with a confidence interval of 0.05 (95%). Results from the regression indicated that rock type and hammer values were strongly correlated to C coefficients (adjusted r = 0.8011), having p values of 0.000 and 0.0024, respectively. Joint width was excluded from the calculation by Statistix 9.0.

In general, results from multiple valley cross-profile data analyses revealed that (1) all sampled profiles could be curve-fitted to parabolas with high r^2 and p (correlation and probability) values, indicating that the morphologies of the study area canyons are indeed parabolas, and (2) that the C coefficient of these parabolic forms are strongly correlated to rock type, and Schmidt hammer values, in that as rock type changes from granite to gneiss, and as hammer values increase, the C coefficient increases (steeper and narrower). A possible explanation of this result is that as rock type changes from coarse grained granite to fine grained gneiss, rock strength increases because of the more homogeneous distribution of minerals in gneiss, allowing for more slope stability at higher slope angles. Schmidt hammer values are also indicative of the compressive strength of rocks, so it is understandable that rocks with higher compressive strengths would be more apt to hold at high slopes following glacial debuttressing.

Detecting variation in cross-valley profiles was complicated, mostly due to the fact that tributary valleys from opposing sides of trunk-streams were rarely symmetrical, that is, a valley on one side of the canyon is not guaranteed to have a counterpart directly across from it, which was also a result found by Seppala (1978). This caused cross-profiles to often have one half that was directly sampling a trunk-stream trimline position, while the other half would be forced to sample a tributary valley, which could be a large, former glacial channel. There were, however, sample sites that afforded cross-valley profiles that sampled both trimline positions. These parabolas, in general, appear to be symmetrical near the tops of trimlines but display less

symmetry as one moves toward the valley floor. This asymmetry has caused all study canyon streams to be (variably) incongruent with the former glacial troughs they occupy, which is basically the result of mass movement deposits.

Management Implications

Slope Failures

Approximately 2.7 million people visited Grand Teton National Park in 2010 (US National Park Service, 2010), and thousands of these visitors use the numerous hiking trails that ascend into the glacially carved, parabola-shaped canyons of the park. It is in these canyons that slope failures occur to an impressive extent, and these failures will undoubtedly have an impact on both hikers and human-built structures such as hiking trails and camping zones (hazards to user safety, damaged or destroyed infrastructure). I urge the GTNP Resource Management staff to explore the detailed map overlays showing slope failures, trails, and camping zones and consider replacing those in danger with new sites away from potential slope failures.

Valley Cross-Profiles

Glacial valley cross-profiles have been shown to be the shape of parabolas by others and again here in my study. Nevertheless, information to visitors (interpretive signs, guidebooks) provided by the National Park Service and others persist in describing them as “U-shaped”. This is an unfortunate choice of terms for deglaciated valleys because it does not describe the true morphology of the form, and because it does not imply genesis either (morphogenetic). A potential replacement, following the needed suppression of the term “U-shaped”, could be *Parabola-shaped or Parabolic valleys.* These are subtle differences in terminology, however, there is truly a distinction to be made. Parabolas, quite simply, are functions in which

$$y = x^2, \qquad (7)$$

where y is the height on the y axis, and x is the height on the x axis, and the tails of the line become asymptotic as x approaches infinity. Conversely, the shape of a "U" is a semi-circle with parallel tails, or "ascenders" (Figure 2.10).

In light of the numerous amounts of past literature describing glacial valleys as parabolic, as well results from this study, I suggest that the term *U-shaped* be suppressed, while concurrently promoting the more appropriate term *parabolic valley* in future literature and park descriptions of glacial valleys.

Acknowledgements

I thank the UW-NPS Research Station, the Association of American Geographers Mel Marcus Fund, and the KSU Geography Rumsey Bissell Marston Fund for sponsoring this research. I also thank the National Park Service for technical support, most specifically Kathy Mellander, Celeste Havener, and the NPS Rangers at Jenny Lake and Moose. Last but not least, I thank Hank Harlow and the crew at the UW-NPS Research Station for their hospitality and assistance with logistics.

Literature Cited

Alexander, D., 1993, Natural Disasters: London (UK), Chapman and Hall Publishers, 255 p.

Augustinus, P.C, 1992, The influence of rock mass strength on glacial valley cross-profile morphology: a case study from the southern Alps, New Zealand: Earth Surface Processes and Landforms, v. 17, p. 39-51.

Augustinus, P.C., 1995, Glacial valley cross-profile development: the influence of in-situ rock stress and rock mass strength, with examples from the southern Alps, New Zealand: Geomorphology, v. 14, p. 87-97.

Benda, L., Veldhuisen, C., Black, J., 2003, Debris flows as agents of morphological heterogeneity at low-order confluences, Olympic Mountains, Washington: Geological Society of America Bulletin, v. 115, no. 9, p. 1110-21.

Brook, M.S., Kirkbride, M.P., Brock, B.W., 2004, Rock strength and development of glacial valley morphology in the Scottish Highlands and Northwest Iceland: Geografiska Annaler, ser. A , v. 86, no. 3, p. 225-234.

Brozović, N., Burbank, D.W., Meigs, A.J., 1997, Climate limits on landscape development in the northwestern Himalyas: Science, no. 276, p. 571-574.

Burchstead, D., Daniels, M.D., Thorson, R.M., Vokoun, J.C., 2010, The river discontinuum: beavers (*Castor canadensis*) and baseline conditions for restoration of forested headwaters: BioScience, vol. 60, no.11, p. 908-921.

Case, J.C., 1989, Wyoming landslide classification scheme: Geologic Hazards Section, Wyoming State Geological Survey: http: www.wrds.uwyo.edu (July, 2010).

Christopherson, R.W., 2009, Geosystems: An introduction to physical geography: Upper Saddle Creek (NJ), Prentice Hall, 687 p.

Cruden, D.M., Varnes, D.J., 1996, Landslide types and processes: *In:* Turner, A.K., Schuster, R.L. (eds), Landslides: Investigation and Mitigation. Transportation Research Board, National Research Council, Washington D.C., Special Report 247, p. 673.

Dackombe, R.V., Gardiner, V., 1983, Geomorphological field manual: London (UK), George Allen Unwin, 254 p.

Davis, W.M., 1916, The Mission Range, Montana: The Geographical Review vol. 2, p. 267-288.

Degenhardt, J.D., Giardino, J.R., Marston, R.A., Pitty, A.F., 2007, Interpretation of a blockstream in Tom Mays Canyon, Franklin Mountains, Texas: Zeitschrift für Geomorphologie, vol. 51, no.3, p. 377-396.

Dixon, D.B., 1906, Easy lessons in mensuration. The National Engineer, Vol. 10(2), p. 31.

English, J.M., & Johnston, S.T., 2004. The Laramide orogeny: What were the driving forces? International Geology Review 46, 833–838.

Foster, D., Brocklehurst, S.H., Gawthorpe, R.L., 2010, Glacial-topographic interactions in the Teton Range, Wyoming: Journal of Geophysical Research, vol. 115, p. 1-20.

Good, J.D., & Pierce, K.L., 2002, Interpreting the Landscape: Recent and Ongoing Geology of Grand Teton & Yellowstone National Parks: Moose (WY), Grand Teton Natural History Association, 58 p.

Graf, W., 1970, The geomorphology of the glacial valley cross section: Arctic and Alpine Research vol. 2, no. 4, p. 303-312.

Harbor, J.M., 1995, Development of glacial-valley cross sections under conditions of spatially variable resistance to erosion: Geomorphology, vol. 14, p. 19-107.

Harbor, J.M., 1992, Numerical modeling of the development of u-shaped valleys by glacial erosion: Geological Society of America Bulletin 104, p. 1364-1375.

Harbor, J.M., Hallet, B., Raymond, C.F., 1988, A numerical model of landform development by glacial erosion: Nature, vol. 333, p. 347-349.

Harp, E.L., Wilson, R.C., Wieczorek, G.F., 1981, Landslides from the February 4, 1976, Guatemala earthquake: U.S. Geological Survey Professional Paper 1204-A.

Hewitt, K., 2006, Disturbance regime landscapes: mountain drainage systems interrupted by large rockslides: Progress in Physical Geography vol. 30, no.3, p. 365-393.

Hirano, M., Aniya, M., 1988, A rational explanation of cross-profile morphology for glacial valleys and glacial valley development: Earth Surface Processes and Landforms, vol. 13, p. 707-716.

Hirano, M., Aniya, M., 1989, Rational explanation of cross-profile morphology for glacial valleys and glacial valley development: a further note: Earth Surface Processes and Landforms, vol. 14, p. 173-174.

Hirano, M., Aniya, M., 1990, A reply to 'a discussion of Hirano and Aniya's (1988, 1989) explanation of glacial valley cross-profile development' by Jonathan M. Harbor: Earth Surface Processes and Landforms, vol. 15, p. 379-381.

Keefer, D.K., 2002, Investigating landslides caused by earthquakes: a historical review: Surveys in Geophysics, vol. 23, p. 473-510.

Lageson, D.R., Spearing, D.R., 1991, Roadside geology of Wyoming: Missoula (MT), Mountain Press Publishing Co., 271 p.

Lawrence, J. D., 2013, A Catalog of Special Plane Curves. United States, Dover Publications, 218 p.

Lisiecki, L.E. and Raymo, M.E., 2005, A Plio-Pleistocene Stack of 57 Globally Distributed Benthic Records: Paleooceanography, vol. 20, no. 1, p. 1003.

Love, J.D., Reed, J.C., Christiansen, A.C., 1992, Geology Map of GTNP, Teton County, Wyoming. Denver (CO): U.S. Geological Society Map Distribution, scale 1:62 500, 1 digital sheet.

Love, D., Reed, J.C., Pierce, K.L., 2007, Creation of the Teton Landscape: A Geological Chronicle of Jackson Hole and the Teton Range: 2nd ed., Salt Lake City (UT), Paragon Press, 132 p.

Mahaney, W.C., 1990, Neoglacial chronology and floristics in the Middle Teton area, central Teton Range, Western Wyoming: Journal of Quaternary Science, vol. 1, p. 53-66.

Marston, R.A., 2010, Geomorphology and vegetation on hillslopes: interactions, dependencies, and feedback loops: Geomorphology, vol. 116, p. 206-217.

Marston, R.A., Miller, M.M., Devkota, L., 1998, Geoecology and mass movement in the Manaslu-Ganesh and Langtang-Jugal himals, Nepal: Geomorphology, vol. 26, p. 139-150.

Mears, B., Jr., 1974. The evolution of the Rocky Mountain glacial model: in Coats, D.R., ed., Glacial Geomorphology, Springer, p. 11-40.

Moon, B.P., 1984, Refinement of a technique for determining rock mass strength for geomorphological purposes: Earth Surface Processes and Landforms, vol. 9, p. 189-193.

Moon, B.P., Selby, MJ, 1983, Rock mass strength and scarp forms in southern Africa: Geografiska Annaler, ser. A, vol. 65, no. 1-2, p. 135-145.

Owen, G., Matthews, J.A., Albert, P.G., 2007, Rates of Holocene chemical weathering, 'Little Ice Age' glacial erosion and implications for Schmidt-hammer dating at a glacier-foreland boundary, Fåbergstølsbreen, Southern Norway: The Holocene, vol. 17, no. 6, p. 829-834.

Patten, R.S., Knight, D.H., 1994, Snow avalanches and vegetation pattern in Cascade Canyon, Grand Teton National Park, Wyoming, U.S.A: Arctic and Alpine Research, vol. 26, no. 1, p. 35-41.

Pierce, K.L., Good, J.D., 1992, Field Guide to the Quaternary geology of Jackson Hole, Wyoming: U.S. Geological Survey Open File Report 92-504.

Pierce, K.L., 2003, Pleistocene glaciations of the Rocky Mountains: Development in Quaternary Science, vol. 1, p. 63-76.

Pierce, K.L., Licciardi, J.M., Good, J.M., and Jaworowski, C., 2018, Pleistocene glaciation of the Jackson Hole area, Wyoming: U.S. Geological Survey Professional Paper 1835, 56 p.

Plummer, C., Carlson, D.H., Hammersley, L., 2010, Physical Geology: 13th ed. New York (NY), McGraw Hill, 644 p.

Roberts, S.V., Burbank, D.W., 1993, Uplift and thermal history of the Teton Range (northwestern Wyoming) defined by fission-track dating: Journal of Earth and Planetary Science Letters, vol. 118, p. 295-309.

Selby M.J., 1980, A rock mass strength classification for geomorphic purposes: with tests from Antarctica and New Zealand: Zeitschrift für Geomorphologie, vol. 24, p. 31–51.

Selby, M.J., 1982, Rock mass strength and the form of some inselbergs in the central Namib Desert: Earth Surface Processes and Landforms, vol. 7, p. 489-497.

Seppala, M., 1978, Influence of rock jointing on the asymmetric form of the Ptarmigan Glacier Valley, southeastern Alaska: Bulletin of the Geological Society of Finland vol. 47, p. 33-44.

Shroder, Jr., J.F., Weihs, B.J., 2010, Geomorphology of the Lake Shewa landslide dam, Badakhshan, Afghanistan, using remote sensing data. Geografiska Annaler, ser A, vol. 92, no. 4, p. 469-483.

Sidle, R.C., Ochiai, H., 2006, Landslides: processes, prediction, and land use: Washington, D.C., American Geophysical Union, Water Resources Monograph 18, 312 p.

Simley, J.D., Carswell Jr., W.J., 2009, The national map—hydrography: U.S. Geological Survey Fact Sheet 2009-3054, 4 p.

Smith, D. E., 1958, History of Mathematics, Vol. II. United States, Dover Publications. 736 p.

Sugden, D.E., John, B.S., 1976, Glaciers and Landscape. London (UK), Edward Arnold, 376 p.

Svensson, H., 1959, Is the cross-section of a glacial valley a parabola?: Journal of Glaciology, vol. 3, p. 362-363.

US National Park Service, 2010, National Park Service visitor summary report total recreation: http:www.nature.nps.gov/stats (March 2011).

Vankat, J.L., 1979, The natural vegetation of North America. Malbar (FL), Krieger Publishing, 261 p.

Viles, H., Goudie, A., Grab, S., Lalley, J., 2011, The use of the Schmidt hammer and Equotip for rock hardness assessment in geomorphology and heritage science: a comparative analysis: Earth Surface Processes and Landforms, vol. 36, p. 320–333.

Wheeler, D.A., 1984, Using parabolas to describe the cross-sections of glacial valleys: Earth Surface Processes and Landforms, vol. 9, p. 391-394.

Wyoming State Geological Survey and the Water Resources Data System, 2001, Preliminary landslide map: Laramie (WY), Wyoming State Geological Survey.

Tables and Table Captions

Table 2.1. Rock mass strength classification, modified from Moon (1984)

	Very Strong	Strong	Moderate	Weak	Very Weak
Intact Strength Rating	100-70 = **20** 69-57 = **19** 56-53 = **18**	52-50 = **16** 49-48 = **15** 47-46 = **14**	43-42 = **13** 41-40 = **12** 39-38 = **11**	37-36 = **10** 35-33 = **9** 32-29 = **8**	28-25 = **7** 24-17 = **6** <17 = **5**
Weathering Rating	Unweathered **10**	Slightly weathered **9**	Moderately weathered **7**	Highly unweathered **5**	Completely weathered **3**
Joint Spacing Rating	>3 **30** | 3-2.2 **29** | 2.2-1.9 **28** | 1.9-1.6 **27** | 1.6-1.4 **26** | 1.4-1.2 **25** | 1.2-1.0 **24** | 1.0-0.8 **23** | 0.8-0.7 **22** | 0.7-0.6 **21** | 0.6-0.5 **20** | 0.5-0.4 **19** | 0.4-0.3 **18** | 0.3-0.25 **17** | 0.25-0.2 **16**	0.2-0.15 **15** | 0.15-0.1 **14** | 0.1-0.07 **13** | 0.07-0.05 **12**	0.05-0.03 **11** | 0.03-0.025 **10** | 0.025-0.02 **9** | <0.02 **8**		
Joint Orientation Rating	>30° into slope **20**	<30° into slope **18**	Horizontal & vertical **14**	<30° out of slope **9**	>30° out of slope **5**
Joint Width Rating	< 0.1 mm **7**	< 0.1-1 mm **6**	< 1-5 mm **5**	< 5-20 mm **4**	>20 mm **2**
Joint Continuity Rating	None continuous **7**	Few continuous **6**	Continuous, no infill **5**	Continuous, thin infill **4**	Continuous, thick infill **1**
Groundwater Rating	None **6**	Trace **5**	Slight **4**	Moderate **3**	Great **1**

Table 2.2. Summary statistics of valley cross-profile analyses.

Table	Mean	Minimum	Maximum	Standard Dev.	Number
Profile Area (km^2)	0.159	0.016	0.586	0.114	44
C Coefficient	0.0018	0.0005	0.006	0.0012	44
Distance to Fault (m)	3035.2	1000	6000	1313.2	44
Form Ratio	0.34	0.23	0.57	0.08	44
Shear Stress (bars)	1.6	0.07	6.9	1.6	44
Weathering	8.07	7	9	1	41
Joint Spacing	18.2	11	28	3.8	41
Joint Orientation	12.1	5	18	4	41
Joint Width	4.3	2	6	1.3	41
Joint Continuity	4.5	1	6	1.2	41
Groundwater	4.8	3	6	0.8	41
Hammer Value	49.1	32	61	8.7	41
Total RMS	67.3	53	78	6.7	41

Figures and Figure Captions

Figure 2.1. View down Garnet Canyon from trail. Note the parabolic valley cross-profile and the rock fall deposits on both slopes.

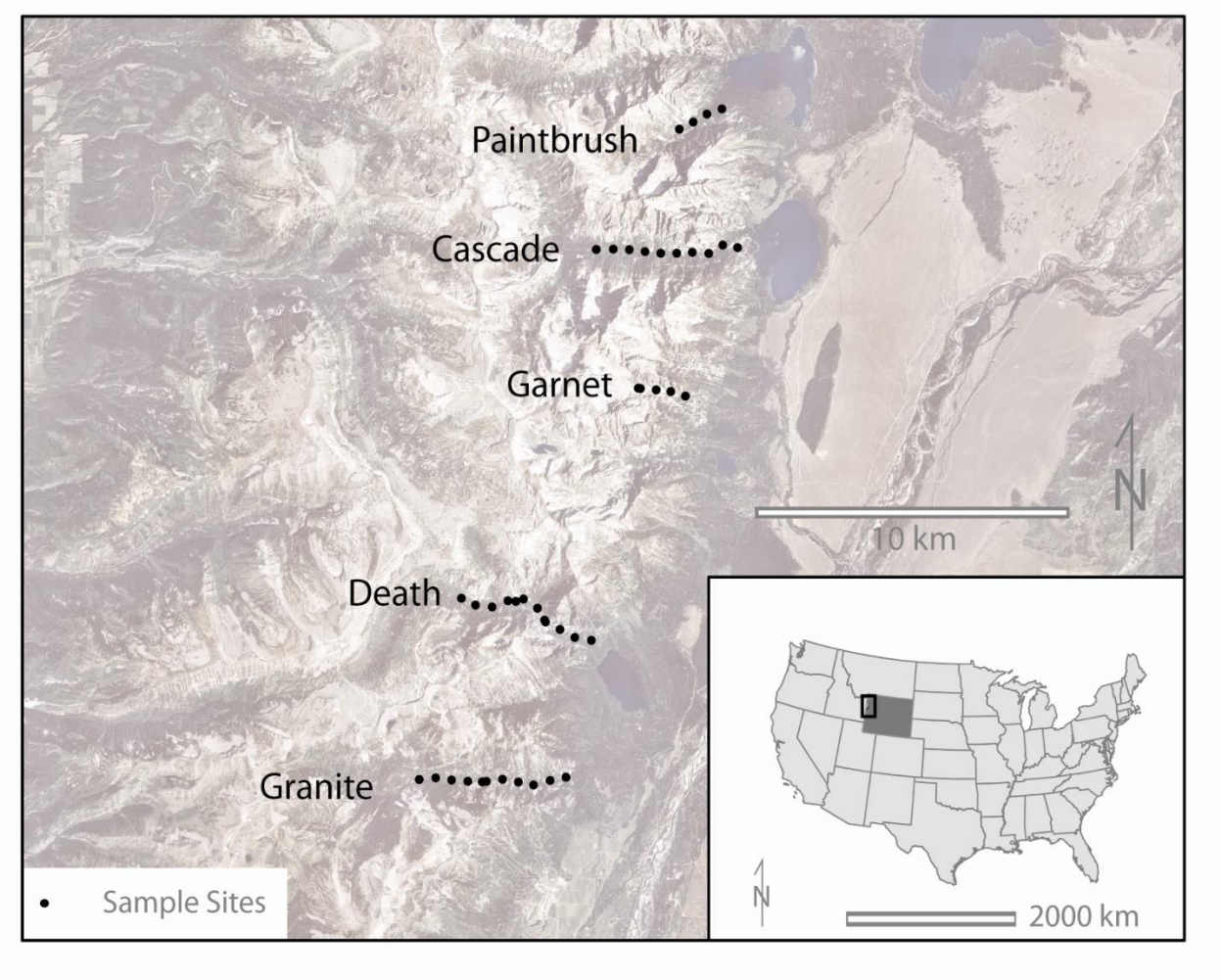

Figure 2.2. Study canyons and sample sites.

Figure 2.3. South-facing slope at site #1 in Granite Canyon. Note the presence of a debris flow intruding directly onto the Granite Canyon trail.

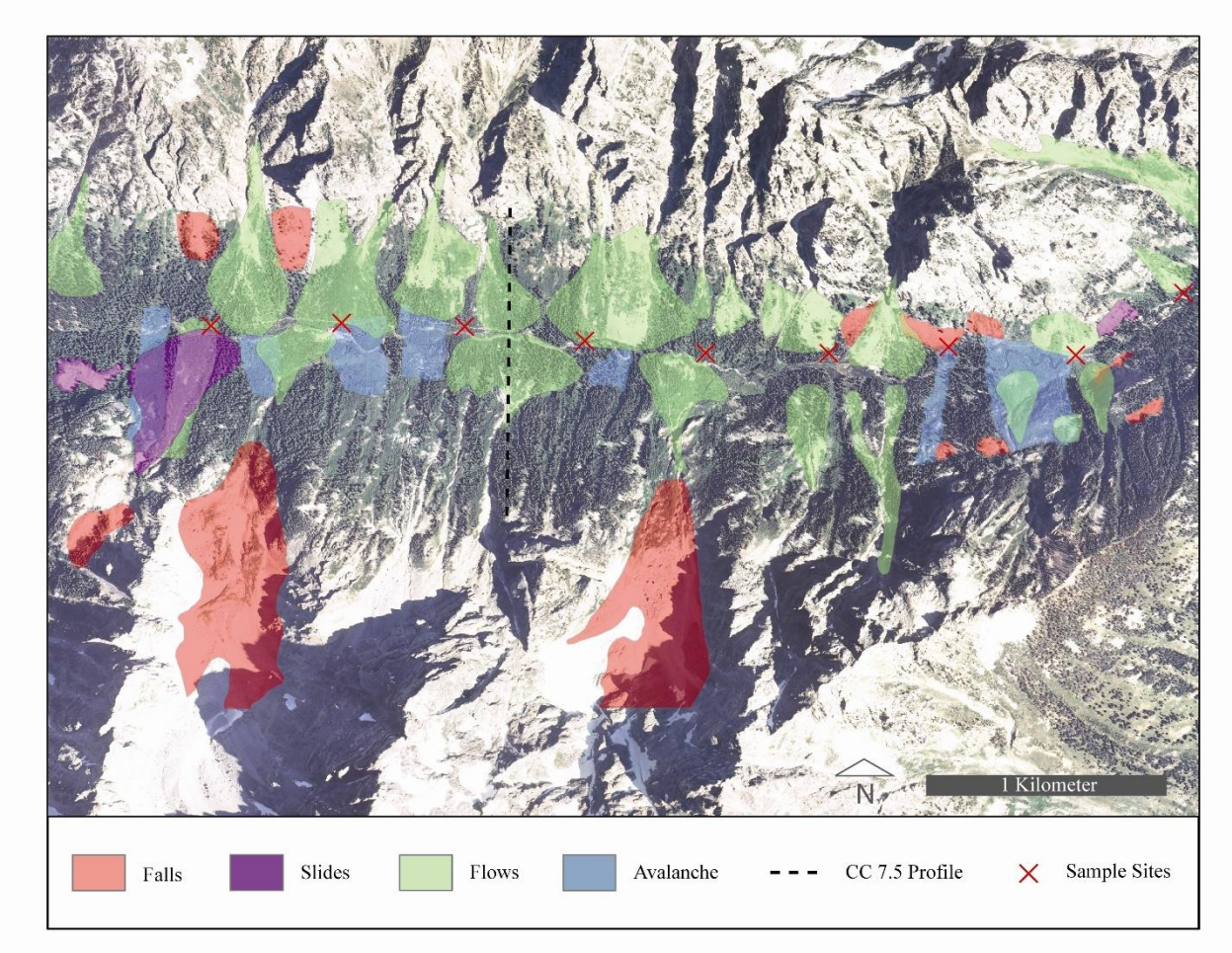

Figure 2.4. Example of a map of slope failures showing all four types, sample sites, and a single profile line in Cascade Canyon. Maps have been created as shapefiles for all study area canyons, provided to the GTNP Resource Management Office.

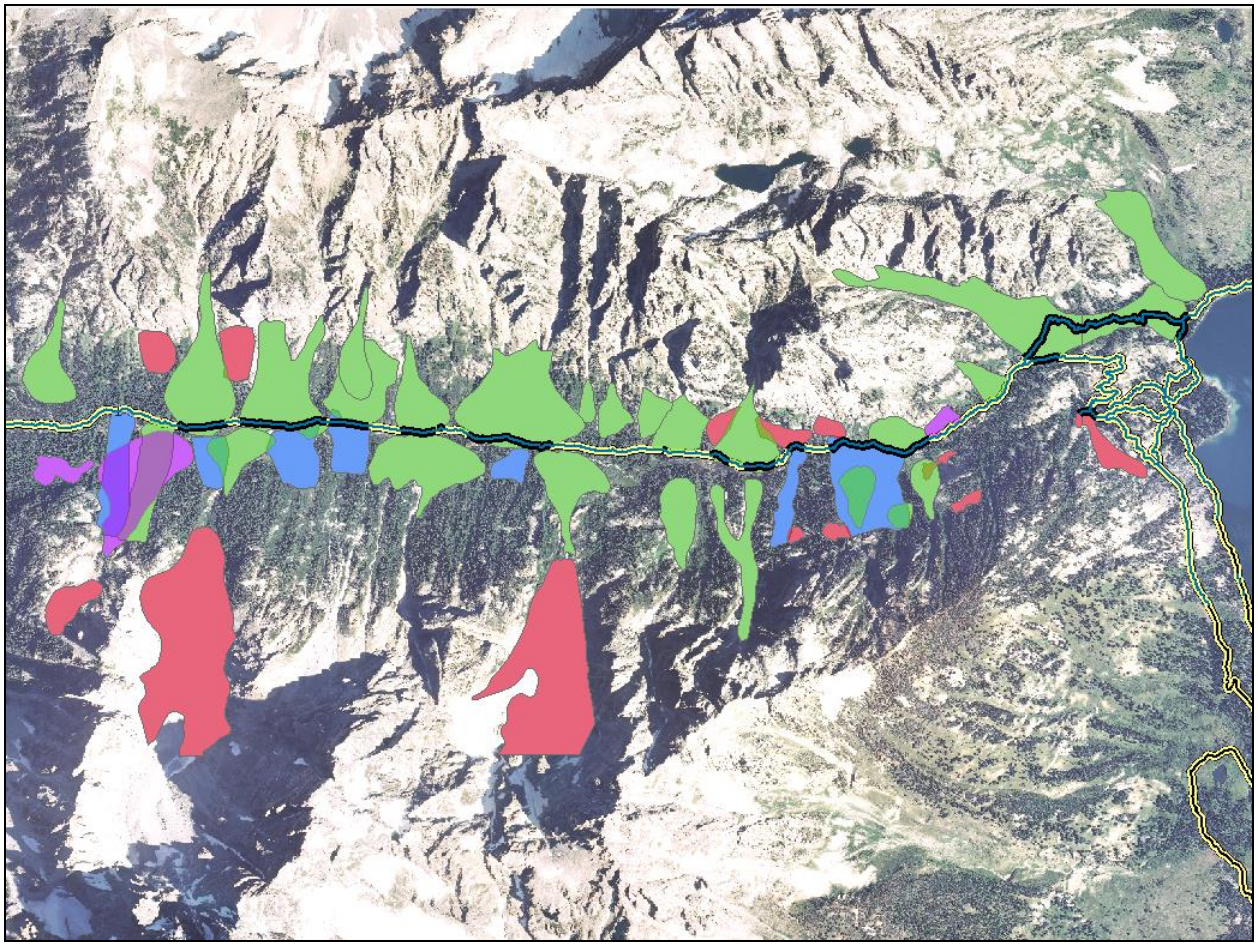

Figure 2.5. ArcMap 9.3 view of Cascade Canyon, GTNP. The black lines represent lengths of trails intersected by slope failure polygons. Green polygons represent debris and rock flows, red polygons represent rock and block falls, blue polygons represent snow avalanches, and purple polygons represent rock and block slides. Yellow lines represent trail segments not directly intersected by slope failures. Similar shapefiles were created for all study area canyons.

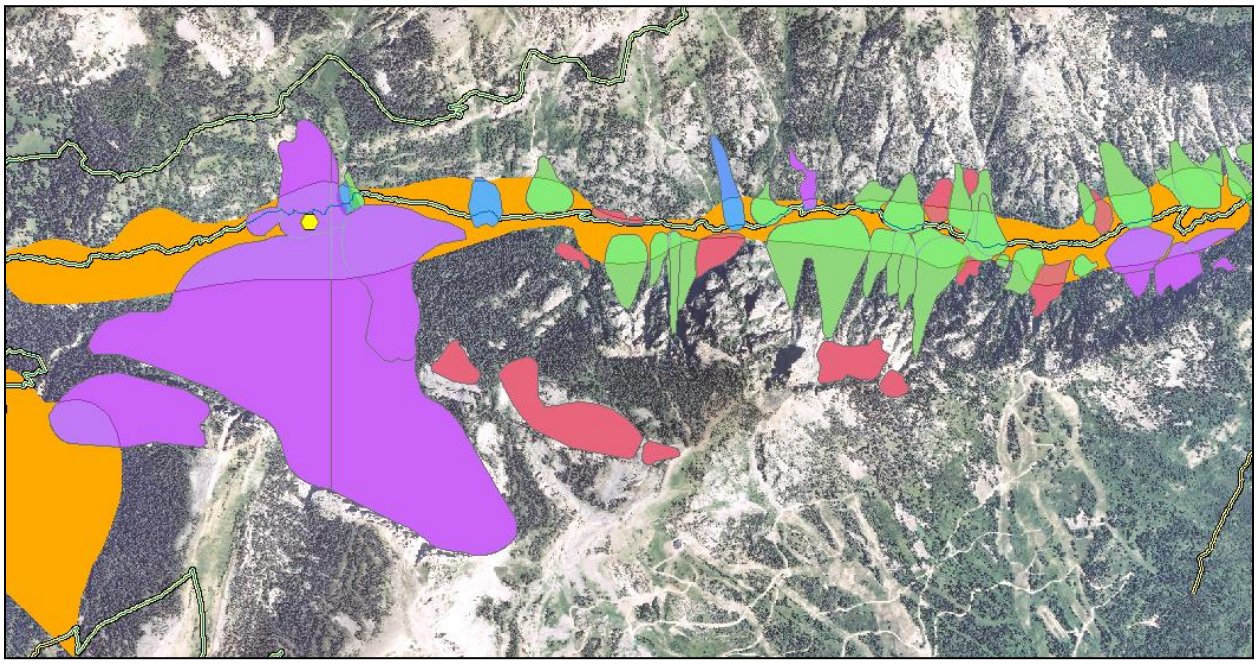

Figure 2.6. ArcMap 9.3 view of camping zones intersected by slope failure polygons in Granite Canyon, GTNP. Orange polygons represent GTNP Camping Zones, green polygons represent debris and rock flows, red polygons represent rock and block falls, blue polygons represent snow avalanches, and purple polygons represent rock and block slides. Yellow lines represent park trails. Similar shapefiles were created for all study area canyons.

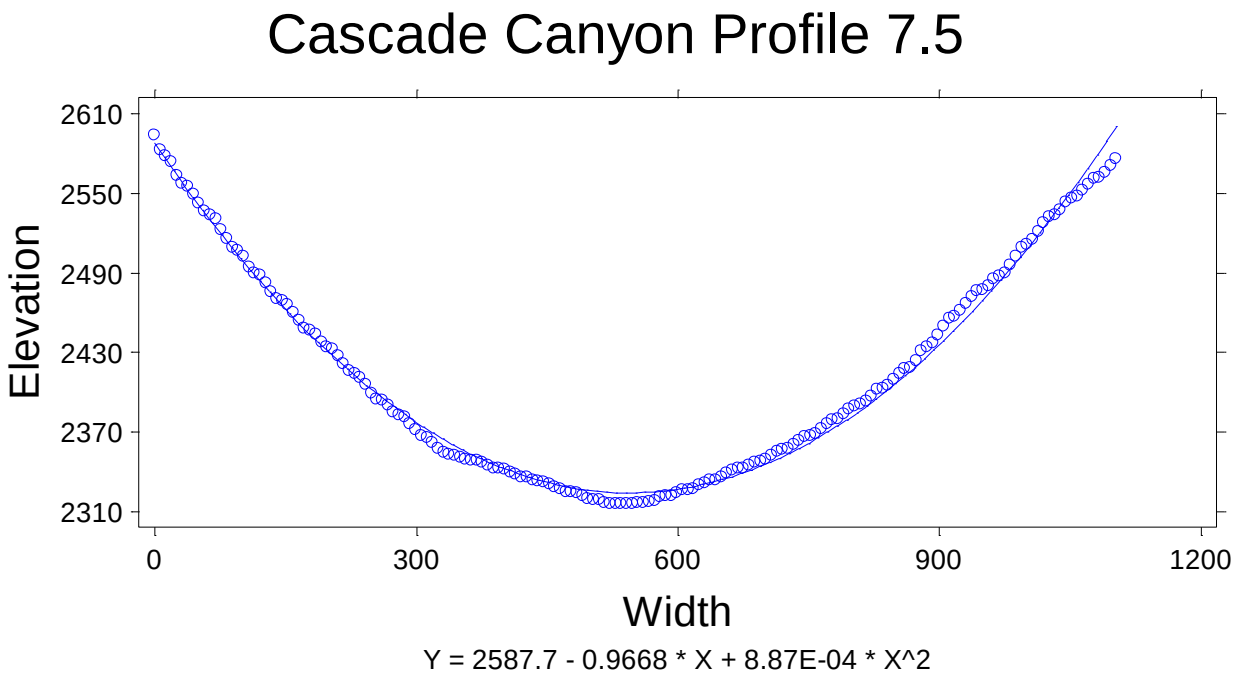

Figure 2.7. Profile elevation data (circles), the regression line (line), and the equation of the regression line for Cascade Canyon, near site 7. Profiles have been created at 44 locations in the study area canyons.

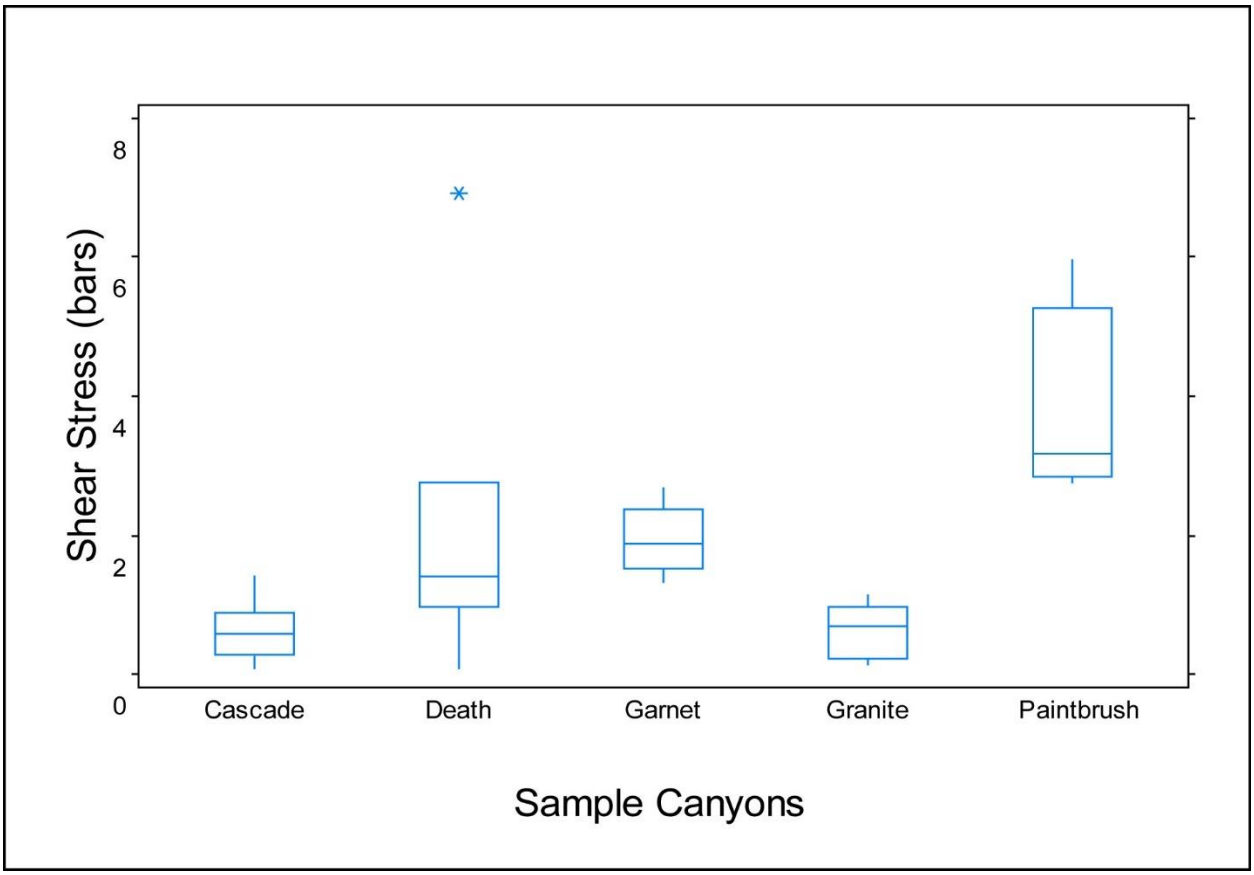

Figure 2.8. Box and whisker diagram of shear stress in the study canyons.

Figure 2.9. Longitudinal profiles of study site canyons.

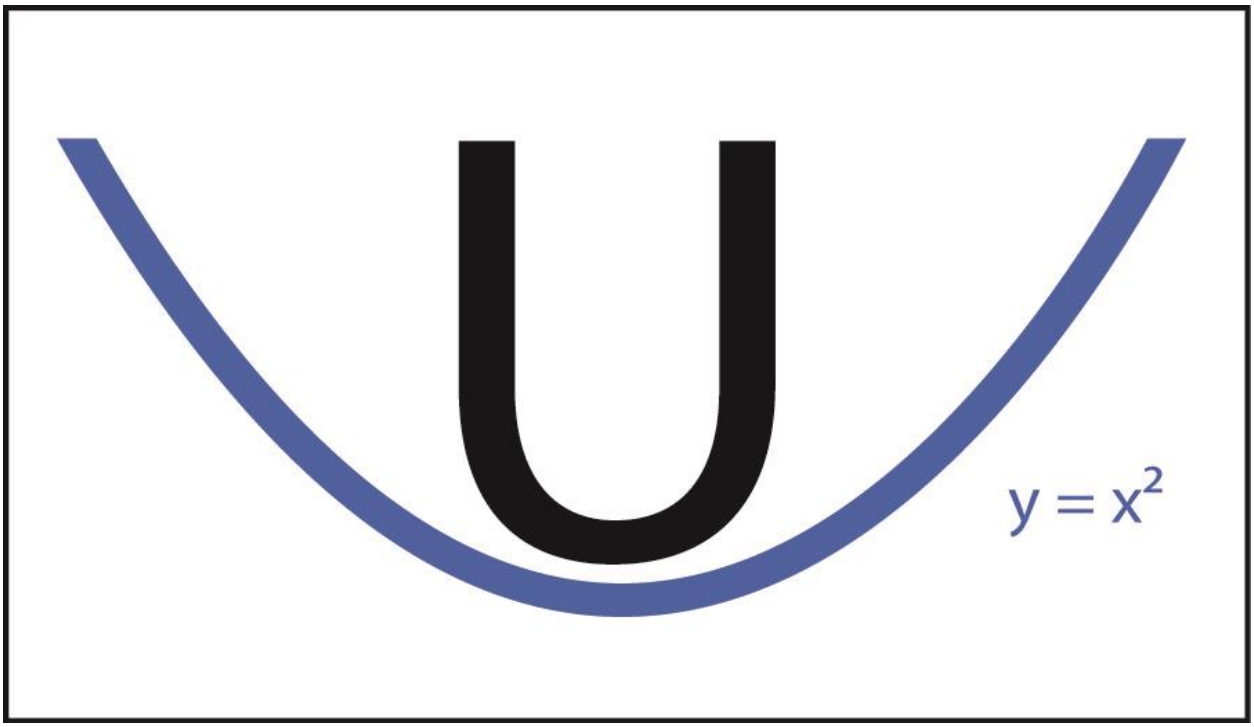

Figure 2.10. U-shaped vs. parabolic valley cross-profiles.

Chapter 3 -

Mass-movement Disturbance Regime Landscapes, Hazards, and Water Implications: Grand Teton National Park, Wyoming

Abstract

The Teton Range is the result of active crustal extension (normal faulting) and is the youngest range in the Rocky Mountains at approximately 2 million years old. The youth of this range, its state of seismic activity, and its recent deglaciation have combined to produce a unique fluvial landscape in that the fault-shattered metamorphic/igneous rocks of the range have been eroding from their source cliffs at high rates which has covered the glacially scoured valley floors with colluvium such as talus slopes, rock slide, avalanche, and debris flow deposits. This project was focused on the characterization of all forms of mass movement, especially rock slides, multiple talus types (rockfall, alluvial, avalanche), protalus lobes, protalus ramparts, lobate and tongue-shaped rock glaciers, and their collective effects on water retention and its late-season downstream delivery in the Grand Teton National Park, WY and beyond. A major goal of this project was to reclassify many of the mass movements in the park in an effort to streamline and simplify previous efforts by other scientists. Methods used during this study included field reconnaissance and measurements acquired during the summers of 2010 and 2013 and measurements taken from various datasets (NAIP imagery, shape files used within a GIS [ArcMap 10.0], and Google Earth™). Mass movement deposits, as well as ice glaciers and long-term snowbanks, were mapped and interpreted. Overall conclusions are that the major sources of mass movements from the Archean crystalline core of the range are the result of extensive jointing, fault-shattering, increased frost-wedging at higher altitudes, slopes steepened by prior glacial erosion, and extensive snow avalanches. Areas of Paleozoic sedimentary rocks marginal to the crystalline core produce rockslides as a result of steep dips and unstable shales beneath massive overlying carbonates. The presence of internal ground ice enables development of

protalus lobes, thicker rock-fragment flows, and thinner boulder streams. Such ground ice is likely to enhance late-season water delivery downstream unless climate warming and recurrent droughts become too extreme.

Introduction

The role of rockslides-rock avalanches in mountain landscapes has been well documented in Himalayan, Alpine, and some Rocky Mountain regions (Hewitt, 2006; Shroder, 1998a,b,c; Shroder and Bishop, 1998; Shroder et al., 1999, 2010, 2011). Although the abrupt slope failures themselves are extremely short-lived events, the persistence of rock-wall detachment scars and the various deposits themselves can persist for long periods as influences on water diversion and impoundment, fluvial and lacustrine sediment retention, sediment H_20 storage as fluid (water) and solid (ice), and the release of occasional landslide lake outburst floods (LLOF). In addition, the more incremental or slower accumulation of collateral mass-movement deposits, such as talus, alpine debris flow cones, snow avalanches, and some rock glaciers and boulder streams with internal ice permafrost also can have both similar and different effects.

The Teton Range is an area of high relief, containing high-gradient drainage and amplified rates of, often catastrophic, colluvial activity. High altitude snowfall (~2 km) is generated as moist Pacific air masses are uplifted over the mountain barrier (Foster et al., 2010). These streams are essentially derived from melt-waters of fresh annual snowpack, firn fields, and remnant glaciers of the late Pleistocene. Because the area is nearly deglaciated, excepting small vestiges of past sizable glaciers (the Teton glacier, etc.), Teton Range trunk-streams are “misfits” or “underfit”, in that they are presently too small to have created the valleys they occupy (Huggett, 2007). Mass movement processes such as debris flows, avalanches, and rockfalls / rockslides occur at extremely high rates in Teton Range. This high-frequency of mass movement is largely due to tectonic and climatic forcing, coupled with the effects of variable rock types and weathering, and post-glacial debuttressing of valley walls. These colluvial processes further complicate the “misfit” fluvial regime with high and frequent debris inputs which overload or even dam streams, causing epicyclical responses (Hewitt, 2006) to the chaotic inputs of mass movement.

This situation of continual or extended disruption of a fluvial regime has been discussed by Hewitt (2006) as a "disturbance regime", which refers to "the long-term or permanent consequences of relatively brief, but reoccurring episodes, usually of high magnitude or at critical sites", which produce landforms "whose location and history are dependent on the disturbances" (Hewitt, 2006, p367). According to Hewitt (2006)(quoting Benda et al., 2003), the landforms of a disturbance regime "tend to be polygenetic and exhibit morphological heterogeneity", also called "patchy heterogeneous morphologies" (Burchstead et al., 2010). Though Hewitt was mostly concerned with mega-scale rock avalanches, or sturzstrom (Shroder & Weihs, 2010), the same phases of the landslide interruption epicycle are observable in Teton canyons.

Teton Range canyons fit under the classification of "a disturbance regime landscape", in that there is an abundance of frequently occurring mass movements that are clearly affecting the centerlines of trunk-streams. It is the primary goal of this paper to describe and explain selected examples of trunk-stream positions in terms of their incongruence with glacial trough centerlines, and the disturbances which have affected their locations in the Teton Range.

Problem Statement

Studies concerning the role of various mass movements and their effects on water delivery are well documented in other ranges such as the Himalaya, or other Rocky Mountain ranges; however, colluvial stream disturbances have not been explained or described for the Teton Range.

Purpose and Objectives

The purposes and objectives of this study were to:

1. Begin with Marston et al.'s (2011) prior funded seminal work for UW-NPS Research Center on cross-valley profiles and mass-movement hazards in deglaciated canyons, Grand Teton National Park (2010), as a fundamental basis for further geomorphological mapping.

2. Apply Hewitt's (2006) methodology for recognizing landslide interruption epicycles in mountain valleys in the Grand Teton National Park; specifically Cascade, Death, Open and Granite canyons (Figure 3.1).

3. Adapt the landslide interruption epicycles of Hewitt (2006) to small discharge canyon streams in Grand Teton National Park as paradigmatic examples of mass-movement control of small-basin alpine drainages (Shroder et al., 1999).

Significance

Mass movements, glaciers, and rock glaciers in GTNP affect water delivery throughout the park, can pose hazards to park users, and are known to create long- and short-term changes in the park landscape. Because mass movements, glaciers, and rock glaciers largely dictate water releases downstream, it is imperative that data be created about their character and the manner in which they affect the fluvial regime. Additionally, because these features are often hazardous to humans, studies that investigate their genesis and continued evolution are warranted in the interest of park safety.

Background

The Teton Range is the result of active crustal extension or normal faulting, and is one of the youngest ranges of the Rocky Mountains. Although movement on the Teton Fault began ~9 Mya, the Teton Range itself is essentially largely Quaternary-aged (i.e. perhaps only ~2 million years old) (Smith et al., 1993; Byrd et al., 1994). Fault scarps and associated stratigraphy reveal Holocene slip rates of 0.45 – 1.6 mm/yr for the Teton Fault that are consistent with a range of recurrence intervals for large, scarp-forming earthquakes of 1600 to 6000 yr. Hampel et al. (2007) have even hypothesized that the post-glacial slip rates on the Teton Fault increased as a result of melting of the Yellowstone ice cap and deglaciation of the Teton range. The influence of high ground accelerations associated with large earthquakes was judged as particularly important in the Teton region by Smith et al. (1993).

Mass movements in the Teton Range are profuse, and much of the valley floors of the range are blanketed by the deposits of various forms of mass movements that occur above

(rockfalls, rockslides, debris flows, avalanche, etc.). Case (1989), in his original aerial photographic mapping of landslides of Wyoming, was able to delineate the greater proportion of the state's slope failures, but given the massive size of the undertaking without enough (or any) field checking for accuracy in mapping, inevitable omissions or errors accumulated. Mass movements come in a great many variable types, which over time, weathering, soil formation, and revegetation, can become obscured as to genesis. The prior work of Marston et al. (2011), which used Case (1989) as an initial base map in five canyons (Paintbrush, Cascade, Garnet, Death, Granite), provides a foundation for mapping of the existing deposits which were omitted/not recognized, misclassified, and/or delineated inaccurately. According to Marston et al (2011), because a propensity of mass movement deposits in GTNP are found below Pinedale glacier trimline positions, glacial debuttressing has played a large role in mass movement deposition since the most recent glaciation. Already in the European Alps, the western Himalaya, and elsewhere degradation of rockwall permafrost is thought to have caused some rock failure such that formerly frozen surficial fracture systems no longer retain bearing strength, thus spontaneously failing (Arsenault and Meigs, 2005; Cossart et al., 2008; Stoffel and Huggel, 2012).

The Pleistocene glacial history of the Teton region has been worked out in fair detail by Pierce and Good (1992), Licciardi and Pierce (2008) and a number of others. Old glaciations, perhaps from the early and middle Pleistocene, are known to have occurred in the Jackson Hole region but their record is poor and whether or not they occurred in the rising but lower altitude Tetons of the time is unknown. The oldest, fairly well understood Munger (Bull Lake?) filled all of the Jackson Hole valley with ice from about 157 to 151 ka, until about 136 ka (Pierce and Good, 1992; Licciardi and Pierce, 2008). Precambrian crystalline rocks from the Tetons in the tills and moraines in Jackson Hole show it is likely that cirques and valleys from the Tetons were also filled with ice at this time. During the succeeding Pinedale glacial, ice advanced from highlands into Jackson Hole from the east, northeast, and north, perhaps because of storms moving up through the Snake River Plain in the Idaho region and building up the Yellow stone ice cap. Glaciers of the Tetons were smaller, although they did join the south-flowing Snake River Lobe of that ice north of Jenny Lake. To the south of there, however, end moraines of valley glaciers from the Tetons extended no more than 2.5 km beyond the mountain front. The precise timing of the Pinedale glaciers from the Tetons has recently been constructed with

cosmogenic dating of boulders and glacially striated bedrock at about 14 ka (Licciardi and Pierce, 2008), but some radiocarbon dates indicate Pinedale ice as late as 9000 yr, perhaps persisting to warm altithermal time around 6000 years ago (Love et al., 2003) when it would have all melted away in most of the lower Teton Valleys. This 14,000- to 9000-year estimation of the melting away of Pinedale ice in Late Pleistocene to Early Holocene time is important because it would be the approximate beginning time for emplacement of the post-glacial, mass-movement debris in the valleys of the Teton landscape. Prior to that time, of course, all mass-movement debris from the valley sides would have fallen on the glacier ice of the time and been transported to the mountain front where it would have contributed to the end moraines encircling the lakes of Jenny, Bradley, Taggart, and Phelps, as well as the mouths of Glacier Gulch and Open Canyon (Love et al., 2003).

The relative youth of the Tetons makes them a particularly useful place to study in terms of landform development and morphology, recent deglaciation, and state of seismic activity, which can be expected to produce significant mass movement through valley wall deglacial debuttressing as the last of the Pinedale ice melted away, as well as horizontal seismic accelerations to the glacially oversteepened valley walls. Foster et al. (2010) noted that the tall, steep hillslopes of the Teton canyons provided shading, as well as plentiful snow influx from avalanching, and insulating debris cover from rockfalls to the valley floor glaciers. Tranel et al. (2011) found that the large talus and mass-movement aprons in some places indicate that the interglacial alpine fluvial system is locally transport-limited and unable to keep pace with the mass movement. The thick mass-movement fans may also enhance chemical weathering of the bedrock beneath them by trapped ground water which would have thereby facilitated periodic glacial incision or fluvial transport during peak flow conditions.

These factors have combined to produce a unique post-glacial, fluvial landscape in that the fault-shattered, metamorphic and igneous, crystalline rocks of the range are being eroded from their source cliffs at high rates that have covered the glacially scoured valley floors with colluvium such as talus slopes, rockslides, avalanche debris, and debris flow deposits. These colluvial deposits have apparently caused the centers of “trunk” stream channels to be variably incongruent with the glacially eroded valley centers.

Study Area

Location

The Teton Range is located in northwestern Wyoming at about latitude 43 º 46’ 46” N longitude 110º 50’ 10” W (~center of range). The range is approximately 72 km long and 20 km wide and is flanked by the south-flowing Snake River ~10 km to the east and by the Wyoming / Idaho state border ~5km to the west (Figure 3.1). The Tetons are the first topographic barrier to moist Pacific air masses moving through the western Snake River Plain (Foster et al., 2010). These conditions favor orographic uplift of moist air masses that in turn drop large (modeled at >2000 mm) amounts of precipitation high in the range Foster et al. (2010). This situation has created “elevated peaks high above the surrounding topography” (Foster et al., 2010), or “topographic lightning rods” (Brozović et al., 1997; Foster et al., 2010).

Quaternary Chronology

The chronology of glacial and other landforming events in the Tetons and Jackson Hole area has been evaluated by a succession of scientists who were impressed with the abundance of glacial, fluvial, mass-movement, and faulted landforms that occur in the area. Plentiful cirques high in the Tetons, glacierized and glaciated valleys with striking parabolic cross sections, prominent terminal and recessional moraines, strong river terraces, extensive and pervasive, polygenetic talus slopes and rockslides, and fresh fault scarps at the front of the Teton Range that truncate lateral moraines; all of these landforms have generated the impressive and iconic landscape of the Grand Teton National Park in western Wyoming. When the first government-sponsored surveys first came to the region from the 1870s to 1900, early researchers noted that glaciers had produced piedmont lakes impounded by morainal material (Bradley, 1973), and the fluvial terraces along the Snake River were related to glacial outwash (St. John, 1877). Blackwelder’s classic work in 1915 established the Buffalo, Bull Lake and Pinedale glacial stages from recognition of moraines near Togwotee Pass into Jackson Hole and glaciated valleys on the north and south sides of the nearby Wind River Range. Fryxell (1930, 1935) then

successfully applied Blackwelder's glacier-stage nomenclature to the Tetons and Jackson Hole area and his application of the terminology has stood the test of time.

Most recently Pierce and Good (1992) and Licciardi and Pierce (2008) carried the Quaternary chronologies forward and updated them with fairly precise cosmogenic exposure-ages of the Bull Lake and Pinedale glaciations in the Teton Range and Jackson Hole areas. One of the primary changes between the older work and the newer is the attribution of a lesser role to glaciers from the Teton Range and an enhanced role to the southern part of the Yellowstone ice mass. Boulders that occur along the southern limit of the penultimate ice advance in Jackson Hole (Munger) give erosion corrected ages of 136±13 ka, with oldest ages of 151-157 ka that correlate with Marine Isotope Stage (MIS 6), as well as with Bull Lake glacial deposits of the Wind River range and West Yellowstone. The timing of the next major glacial advance in the region is the Pinedale (MIS 2) with maxima varying from ~18.8 to ~16.5 ka, to possibly 14.6ka around the southern margins at Jenny Lake. Late Pinedale events in the Teton – Jackson Hole region suggest that major advances or stillstands of a large valley glacier from the east flank of the Teton Range occurred after the global Last Glacial Maximum (LGM) just prior to the Younger Dryas (roughly between 11.5 to 13 ka)(Pierce, 2003), followed by full and rapid deglaciation of the whole Yellowstone Plateau. An important observation is the strong climatic gradients observed between the floor of Jackson Hole to the east and deeper into the mountains to the west as a reflection of the westerlies and the resulting rain-shadow gradients. For example (Pierce and Good, 1992), the mean annual precipitation at Jackson is only about 4.3 cm, whereas only 10 km west at Wilson it is about 10 cm.

Methods

Field Reconnaissance

Each mass movement deposit visited in the field was visually observed and photo documented. For some deposits, such as the Rendezvous rockslide, observing both the headscarp and toe was possible (because it was accessible), providing more comprehensive field data for those deposits. Slope angles of deposits were measured using an Abney hand level where

vegetation was permitting. Dipping strata were measured with a Brunton pocket transit. Water output from mass movements was measured qualitatively where possible, such as return flow from a landslide's toe.

Geomorphological Mapping

Combined with data collected in the field, geomorphological mapping was concluded in the laboratory using ArcMap 10.0. Several data were used to map/delineate and describe landforms under study. These data included (but were not limited to):

- National Areal Imagery Program (NAIP) imagery (2012, 2009) ~1m resolution
- National Elevation Dataset (NED) ~10m resolution
- Geologic Map by Love et al. (1992)
- Landslides of Wyoming shapefile by Case (1989)
- Google Earth™ imagery

In general, field and lab-discovered mass movements, protalus lobes, glaciers, rock glaciers, and slow rock fragment flow deposits were digitized using NAIP imagery and aided by Google Earth™. The digitized outputs (a shapefile) were then populated with attribute data such as mean elevation and mean deposit aspect. This attribute data was subsequently used in Excel 2010 to produce summary statistics of the various deposits.

Landslide Interruption Cycle Identification

The Hewitt (2006) landslide interruption cycle of five phases, each with variable sediment assemblages, constitutes the *landslide-interrupted valley landsystem,* which will be utilized as the theoretical background for the primary mapping tool. As Hewitt (2006) has noted, this type of landsystem creates naturally fragmented fluvial systems in which a *disturbance regime geomorphology* can be identified. The five phases to be identified are: (1) *Landslide complex*, with associated mass movement emplacement forms (rock slide, rock fall, debris flow, etc.) (Shroder et al., 2005); (2) *Impoundment complex*, with associated aggradation and constructional landforms upstream of the barrier, and possible downstream erosion and/or

sedimentation; (3) *Degrading interruption complex*, with trenching and removal of the impoundment complex and downstream sedimentation; (4) *Superimposed interruption complex*, with exhumation of buried valley fill and incision into pre-landslide valley floor; and (5) *"Shadow" interruption complex*, with minor but persistent legacies of interruption, mainly bedrock forms.

The application of Hewitt's (2006) landslide interruption cycles to landforms in the Teton Range involved:

- Modifying of the landslide interrupted valley landsystem to reflect the different nature of the Teton mountain valleys from those in the western Himalaya with large-discharge rivers in them where the landsystem categorization was first developed.

- Differentiating landslide impoundments from paleo-beaver dam impoundments, or even paleo-beaver dam modification, or augmentation of a prior mass-movement impoundment.

- Mapping the locations of streams running over bedrock, as opposed to other kinds of sediment covering bedrock where possible in the field.

- Differentiating between the kinds and sources of the sediment covering the bedrock.

Preliminary Results & Discussion

Geomorphological Mapping

Efforts to expand and correct/reclassify previous mapping done by Case (1989) and Marston et al. (2011) resulted in many new, or corrected, delineated deposits. This study identified 57 features (glaciers [10], rock glaciers [20], protalus lobes [22], slow rock fragment flows [3], rockfall talus [1], and a single slump block). Some of these features were not previously mapped by Case (1989) or Marston et al. (2011) (2 protalus lobes and 1 rock glacier). There were also some features from Case (1989) that required reclassification based on field and laboratory findings. These reclassifications were performed for protalus lobes, rock glaciers, and slow rock fragment flows that were purported by Case (1989) to be something different. In total,

there were 12 deposits in which there were discrepancies between Case's (1989) and this study's findings. Because of the use of DEMs, high resolution imagery of various dates and digital globes such as Google Earth™, my findings are more resolute than Case's (1989) work, which was limited by the use of aerial photography and sporadic fieldwork, if any.

Landslide Interruption Epicycles

My preliminary assessments of the canyons selected for this study indicate a number of examples of phenomena which will be useful in applying the Hewitt (2006) designations. For example, Phase One (emplacement) and Phase Two (impoundment) can be observed in Cascade Canyon where a debris flow has impounded a small lake behind it (Figure 3.2) and at the Rendezvous Rockslide (Figure 3.4). This is echoed by other similar mass movement-generated impoundments in Leigh (Figure 3.3) and Moran Canyons. In other cases, either limited time since emplacement of the landslide, or limited discharges may have precluded significant downcutting and lateral erosion to take parts of the valleys into the more advanced stages of Hewitt's classification scheme. The Rendezvous Rockslide in Granite Canyon (Figure 3.4) may fit some of the criteria for Phase Four in that the impoundment area has been drained and slightly incised; however, the incision is limited to the lake sediments and not the bedrock beneath. No evidence of Phase Five (epigenetic gorges) was observed during this study. It is likely that the scales of Teton processes (such as mass movements and water discharge) and time since the most recent deglaciation have not been of sufficient magnitude to produce the landforms that Hewitt (2006) found in the much older and larger-scale Himalayas.

Rendezvous Rockslide

The Rendezvous Rockslide is a large slope failure on the northwest-facing side of Rendezvous Mountain above Teton Village near Jackson Hole, WY. It can be accessed from the top by an arduous and dangerous descent from the tramway ride stop at the top of the ski area, or from the trail up Granite Canyon to the toe of the failure in Granite Creek. The slope failure

descends from an altitude of about 9600 feet (2925 m) on a generally northwestern trajectory, down to an altitude of about 7880 feet (2400 m) in Granite Canyon, which is a descent of about 1720 feet (525 m) vertically downward in about 1.2 mi (2 km) downslope (Figures 3.4 & 3.5).

The bedrock geology map of the region (Love et al., 1992) shows that the direct or proximate cause of the landslide was the presence of the massive carbonates of the Gallatin Limestone, Bighorn Dolomite, and the Darby Formation that occur above and overload the unstable Park Shale Member of the Gros Ventre Formation (Love et al., 2007). The combination of the weight of these overlying formations totaling some 980 feet (300 m) of thickness, as well as the ~20° angle of dip to the northwest down into the Granite Canyon valley, and the abundant precipitation and high freeze and thaw of the mountain environment have combined to produce the slope failure.

The uppermost main scarp of the slope failure at the top of the Rendezvous Mountain ridge has been eroded down to a low rounded ridge at about 9560 feet (2914 m) that is only about 160 feet (48 m) high, but on the nearby left (west) flank of the landslide the huge cliffs of Gallatin Limestone, and Bighorn Dolomite rise some 600 feet (180 m) above the surface of the landslide, where major rock blocks have been provided to the failure. Furthermore, about halfway down the lateral west margin of the landslide, a second major lateral scarp cliff of dominantly carbonate rocks of the Darby Formation also rises a similar amount in huge cliffs.

The overall surface of the landslide mass is a hummocky rolling terrain, with several undrained depressions, one of which holds an intermittent small lake and grassy area in the upper third of the mass, about 580 m down from the top of the slide. The depression appears to hold water for at least part of the year as a result of the presence of impermeable shale remnant masses that outcrop around the depression. The landslide measures about 2 km in length and is about half a km wide in the middle and lower sections, although it is only about 0.2 km wide at the narrower top. The uppermost part has a considerable amount of remnant shale exposed in heaps and mounds where it has been forced by the presumably repetitive slope movements. The lower two thirds of the landslide mass have plentiful large boulders, ten of which were measured on Google Earth™ and found to average ~21 m in diagonal long axis. Midway down the slope failure on the left (southwest) flank where a change in movement direction occurs from WNW to NW, two offsetting shear planes daylight at the margins to form two stepped terraces, each about

10 m high, the risers of which are the surface manifestation of the shear planes. It is apparent that the main mass of the slope failure has subsided here to show the shear planes.

The lowermost toe of the Rendezvous Rockslide is estimated to be at least 60-80 m thick (perhaps thicker), and appeared to be comprised of at least two main episodes of movement, one above and overriding the other. The lowermost part of the toe was composed of large boulders, the interstices of which appeared filled with weathered debris and soil, whereas the uppermost part of the toe appeared to have a dominance of open matrices, with far less weathering degradation. This lowermost and apparently older toe is conspicuous in having a plentiful forest cover of large, old-growth conifers that are well-rooted in the weathered soils that have developed throughout the lower portion of the mass. Although no date estimates could be obtained from soil thickness measurements in the limited time available for investigation, it is possible that these two movement lobes may represent dominant movement during times of greater precipitation and/or permafrost degradation at the end of the Pleistocene or early Holocene. Presumably, the slope failure would not have been active because it was frozen during Pinedale glaciation and any prior mass movement would have been removed by glacier ice in Granite Canyon, but in the subsequent melting away of Pinedale ice, and the unstable climate associated with the Little Ice Age in late Holocene, other movement could have occurred.

The Rendezvous Rockslide was low velocity as it moved slowly and most probably intermittently down into Granite Canyon but did not climb the north side of the canyon at all. In all probability the mass was comprised of many small and independent motions that collectively brought successive masses of rock fragments of the Paleozoic rock fragments to lower positions in the valley over multiple years of rock motion, more in wetter years, and less in drier. The hydraulic associations of the Rendezvous Rockslide are unknown, although it is likely that almost all of the precipitation that falls upon the feature infiltrates downward through the profuse open porosity between the plentiful boulders and becomes groundwater. Much of this water would have been absorbed by the shales lower down and contributed to their plasticity. The basal slip surface(s?) of the landslide appear to be largely on the uppermost Death canyon Limestone Member of the Gros Ventre Formation.

The overall slope of the outer landslide surface is about 13°, which compares with the generalized dip of the bedrock at this location of ~20°. The ~7° difference in amounts can be explained by the landslide accumulating mass in the valley below, which would reduce the

overall surficial gradient. It is thus apparent that the cause of the slope failure was the incompetence of the Park Shale, which permitted the motion of the landslide to run largely along the bedding planes at the top of the Death Canyon Limestone. This latter rock unit forms a prominent planar shelf of resistant bedrock that is characteristic of much of the high topography elsewhere on Rendezvous Mountain (shown in Figure 30 of Love et al., 2007), as well as the head of Death Canyon, where it forms a prominent landform of conspicuous size that is known as the Death Canyon Shelf. This feature extends southwest-northeast laterally within the Grand Teton National Park for over 5 km, averaging some 300-400 m in width with conspicuous rockfall talus and protalus lobes along it with conspicuous rockfall talus cones and protalus lobes and ramparts that have developed from the rock fragments emanating from extensive freeze and thaw of the rock cliffs of Big Horn Dolomite and Darby Formation rocks outcropping along it.

The toe of the Rendezvous Rockslide partially blocked the course of Granite Creek that runs in the bottom of Granite Canyon, which caused upstream aggradation and the deposition of a flat plain of finer clastics (gravels, sands, silts, and clays). The aggradational plain extends upstream for ~450m and ~200 m in width and is covered with sedges, grasses, and willows in between the multiple channels of Granite Creek that have developed over the aggradational plain. In the bottom of Granite Creek stream channel, swirls of ascending sand-grain plumes attest to water under pressure from below that is rising into the channel from shallow groundwater base flow that comes in from uphill water sources, probably from both sides of the canyon; landslide source on the southwest side, as well as the opposite northwest side where water can also infiltrate into the low gradient slopes there.

The Rendezvous Rockslide is a reasonably typical type of slope failure that is fairly characteristic all-over various parts of Wyoming in other uplifted mountain terrains where the carbonates and shales of the Lower Paleozoic produce similar mass-movement landform features. For example, at the head of Shell Canyon in the western Bighorn Range, a similar suite of rocks has produced even larger and more pronounced failures of the bedrock, with extensive glide blocks, rockslides, and slow-flow features under similar structural conditions of dipping carbonates and shales at moderate to higher altitudes.

Alpine debris cones and fans

The alpine debris cones and debris fans emplaced in the many canyons of Grand Teton National Park have been formed by a variety of processes that require considerable elucidation to delineate process and form in such a fashion as to serve as explanatory templates for similar assessments in other mountain ranges. Certainly such work has been undertaken in many other environments such as in the European Alps, the Canadian Rockies, the Colorado Rockies, the Himalaya, and elsewhere, but still a refresher look at the features can be instructive, particularly where common polygenetic overprinting of process and form can cause misinterpretation. All of the alpine mass movement forms can constitute a variety of talus accumulations that originate solely, or by some combination of falling rock fragments, running water from rainstorms or snow melt on mountain slopes, or by snow avalanches (White, 1981). These accumulations of alpine debris form in cones or fans at various angles of repose, from the steep ones at >35° - 45° for rockfall talus, to 35° - 38° for the upper slopes and <28° for the talus toes of alluvial talus, and <25° for avalanche talus, which also has gently concave-up toes where the snow avalanches sweep out. In addition, talus subtypes occur of the more strongly developed avalanche boulder tongues or avalanche roadbank tongues, and the protalus ramparts with rock fragments that move out over snow banks to pile up as ridges at the base of talus slopes (White, 1981). All of these constitute what can be quite polygenetic forms of alpine talus that is emplaced in what has been considered a reasonably non-catastrophic fashion, wherein most of the rock clasts come down as isolated unit rockfalls and slides, or are emplaced by snow avalanches, or by isolated rivulets in rainstorms (Figures 3.6 & 3.7).

This reasonably non-catastrophic emplacement is contrasted with the truly catastrophic, very rapid, and large forms such as the larger rockfall debris streams, rock avalanches, or sturzstroms, rock slides, debris slides, or the large slump-earthflows and large slow debris flows that are so characteristic of areas with extensive and weak sedimentary rocks. The Teton Range has a sedimentary rock cover of Lower Paleozoic shales and carbonates to the west and south that lap onto the Precambrian crystalline rocks at the core of the upfaulted block that constitutes the highest portions of the range (Figure 3.8). These sedimentary rocks, with their unstable shales beneath massive carbonates, are the main source of rock rubble that makes up the widest variety of mass movement in the outer fringes of Grand Teton National Park. In the high core of

the range, however, the crystalline rocks of gneisses, granites, amphibolites, metagabbros and the like are not as conducive to the formation of large mass movements as are the less stable sedimentary rocks, but still the extensive jointing, fault shattering, steep slopes, and higher altitudes that promote considerable freeze and thaw can also contribute large quantities of rock rubble that are commonly remobilized into extensive talus cones and fans, as well as the glacier moraines, rock glaciers, protalus lobes, and the like that characterize much of the range. Unlike the Himalaya and Hindu Kush where the relief and steep slopes are so much greater and high seismicity and massive rock avalanches from crystalline rocks abound (Shroder and Weihs, 2010; Shroder et al., 2011), large rock avalanches have not been mapped in the Tetons, although a variety of large failures of sedimentary rocks are known. The nearest known seismically induced rock avalanche or rapid rockslide was the one across the Madison River in 1959 125 km NNW of the Teton Range that was produced by a magnitude 7.5 earthquake. The well-known Gros Ventre Rockslide of 1925 that occurred just 20 km east of the Teton Range was caused mainly by increased shear stress exerted from excess snowmelt and rainwater loading, coupled with the Tensleep Sandstone overlying Amsden shale dipping into the Gros Ventre River valley where the river had previously undercut the slope and thereby reduced shear resistance. Numerous other slumps, slow debris flows and earthflows are known in the general region as well, mainly from combinations of weak and dipping sedimentary rocks and plentiful precipitation that loads slopes with heavy surcharge weights, dissolves cements, causes extensive freeze and thaw, brings in seepage pressures, and causes friable shale to lose strength, which collectively results in many slope failures.

Glaciers and Rock Glaciers

Glaciers are masses of permanent snow and ice that move slowly downhill under the influence of gravity, and rock glaciers are similar masses of ice that are completely or largely covered with rock fragments, which obscure the ice cores or interstitial ice cements beneath. Rock glaciers are distinguished from other forms of alpine debris by having steep fronts at the angle of repose that are caused by the top moving faster than the base, with the result that the rock fragments pile up steeply at the front Giardino et al. (1987). The formation of glaciers

occurs as winter snows accumulate to such an extent that all of the winter's accumulation does not melt entirely away each summer, and instead some snow converts to crystalline firn or pellets of ice that last through the melt season into the next winter. After the passage of some 3 – 5 years, the mass of stored ice can become sufficiently large so as to begin flow downhill as an ice glacier. Rock glaciers can begin formation as either masses of rock fragments into which meltwaters drain and refreeze to reconstitute as interstitial ice cements. They can also begin as masses of snow and ice in snow banks, or even ice glaciers that become covered with so much rock debris that the original snowbank or glacial origin can be lost and the masses come to move downslope through various causes of freeze and thaw or permafrost creep, but always with steep fronts of rock fragments at the angle of repose. Talus slopes can fill with such expanding interstitial ice to bulge out at the bottom as protalus lobes, which if developed to an extent that the projection of the talus slope down to the horizontal is greater than the projection of the lobate front down to that same plane, then the feature is considered to be a protalus lobe, but if the lobate front bulges out and travels further than the projected talus extent, then the feature is a lobate rock glacier (Figure 3.9). On the other hand, the ice-cored rock glaciers can commonly form from the overall downwasting of the ice glaciers until all, or almost all of the original ice is covered up and the true glacial nature of the feature is lost. A renewal of cold temperatures or development of greater refreezing of the down-trickling meltwaters from snow melt or the like can then cause the ice core to push the terminus of the feature forward again so that a steep front of rock fragments at the angle of repose develops, at which point a tongue-shaped rock glacier with an ice core has formed.

Because both glaciers and rock glaciers represent ice resources stored away for different amounts of time until finally melted, they constitute important sources of meltwater when finally converted from solid into liquid at some point in their history. Thus, in Grand Teton National Park, it is important to better understand the hydrologic cycle as it is constituted in the region, especially if this hydrologic cycle changes greatly in coming years due to climate warming and drying.

Most of the glaciers recognized in the Teton Range have a north or east aspect, with the exception of Falling Ice Glacier on Mount Moran, which faces to the southeast. All these recognized ice glaciers occur on the east side of the range (Fryxell, 1935), which is no doubt due to primarily to the westerly winds that blow snow over the range to form east-facing cornices

that avalanche down to form the glaciers on that side, as well as to decreased solar radiation on the east sides of the range as the sun is more intensive late in the day in the west. Many of the tongue-shaped rock glaciers on the high peaks of the Teton Range, on the other hand, occur on the west and north sides where snow does not accumulate as much as to the east, although the rock fragments from high freeze and thaw are still abundant, and the altitude is great enough and the topographic and rock-fragment shielding is enough so that the ice does not melt away (Figure 3.10). These tongue-shaped rock glaciers show by their occurrence in deep cirques that they were indeed once ice glaciers, and their lobate nature, with many longitudinal ridges and furrows and steep fronts at the angle of repose show that they remain active.

Glaciers in the Teton Range were first missed by the early explorers in the Hayden surveys of the 19th century, but later in the 20th were noted and described by a variety of people (Fryxell, 1930, 1935; Reed, 1964, 1967; Edmunds et al., 2011), but because most are small and not the lengthy and impressive ice masses of the polar regions or the high alpine ranges of the Himalaya and other famous ranges, the Teton glaciers have been considerably discounted by many. Devisser (2008) has noted that in the Tetons, roughly 276 permanent snow and ice bodies occur with a minimum elevation of 2694 m, a maximum of 4096 m and an average of 3127 m, and a total combined area of 6.9 km ^{2}. Many of these are immobile snowfields, not true, moving glaciers. The Teton Range does contain 10 of Wyoming's named glaciers, the largest of which is Teton Glacier, which Devisser (2008) calculated at 0.30 km^2, but Edmunds et al. (2011) noted its diminution successively from 1967 at 0.258 km^2 to 2006 at 0.215 km^2. Edmunds et al. (2011) also assessed Middle Teton Glacier and Tepee Glacier for the same time period and noted collectively that the greatest loss of glacier mass occurred from 1983 to 1994, which coincided with a rise in temperatures and a reduction in snowpack. The rock glaciers of the Teton Range are largely unnamed and unstudied, which is unfortunate because they do represent a fair amount of unaccounted for permafrost ice that most likely provides considerable late summer – early fall meltwater overland flow and groundwater base flow into the mountain streams.

Management Implications and Conclusions

Teton Range Mass Movement Interruption Epicycles

This study shows that the Teton Range contains evidence of Hewitt's (2006) landslide-interrupted valley landsystem classification. Most impressively, the Rendezvous Rockslide and its subsequent impoundment of the lake below are regional exemplars a phase (3)-degrading interruption complex, and indicates the landslide interruption process is not spacio-temporally scale dependent. In other words, differences in scale (time and space) between the Himalayas and the Tetons is not prohibitive of generating similar landforms. As discussed, the youth of the Tetons, recent deglaciation, and competent basement rocks have combined to produce the glacially-incised, over-steepened valleys with currently (Holocene) failing walls in the absence of ice buttressing which has generated the conditions leading to the phases of landslide-interrupted valley landsystems.

Mass movements, Rock Glaciers, and Glaciers as Water Retention Features

Results of this study confirm and reiterate that mass movements, rock glaciers, and glaciers in GTNP attenuate water at up-elevation locations, and arguably for years to centuries depending on the feature. These landforms then, affect the local hydrologic cycle, and perhaps dramatically, through the lag and pulse effects of stored or mobilized water downstream, respectively. This situation has the potential to exacerbate the ever-present, cascading, trophic effect on most biota in the absence or abundance of water as climate change continues to cause weather extremes. Monitoring of precipitation and stream discharge at plentiful locations throughout the park would help future scientists better untangle the influences of landform classes or individual features on water distribution in GTNP.

Lack of Gauges in GTNP Streams

At present, there are no water discharge recording stations in GTNP streams. This situation impedes long term monitoring of the quantity and timing of up-canyon water attenuation and release. Adding these gauges would benefit further investigations of the water resources in that having baseline data of water availability would help ensure correct management treatments be used to secure floral and faunal assemblages, as well as any ecosystem services supported by water. Additionally, streams in Grand Teton National Park are undisturbed (anthropogenically) and so these "pristine" waterways could serve as benchmark streams for unmodified water delivery system studies; a practice of the U.S. Geological Survey.

Future Hazards to Park Visitors

While it is fairly impossible to "predict" individual mass movements with any certainty, (sans the precursors to an imminent failure like ground cracks) the ability to recognize areas more prone to failure is likely a more fruitful pursuit. Because the geologic contact (unconformity) between the Archean crystalline rocks and Paleozoic sedimentary rocks of the range creates a situation of comparatively more labile, or "weaker" rocks, at the margins of, and inside the canyons of GTNP, prudence should be exercised in not placing campgrounds and hiking trails on or near such areas where, for example, daylighting sedimentary rocks are overlying crystalline basement rocks.

Nomenclature of Teton Landforms

While a vast majority of the landforms in GTNP are properly classified, this study has uncovered several instances in past studies where a feature has been incorrectly classified. In doing so, I have reclassified any landforms whose character does not match the textbook

description of the feature. This may have implications to park managers in terms of signage, or park information provided to the general public.

Acknowledgements

I thank the UW-NPS Research Station and the Association of American Geographers Mountain Geography Specialty Group Chimborazo Fund for partial funding of this project. I am very grateful for everyone's logistical assistance and hospitality at the research station, notably Dr. Hank Harlow and Celeste Havener. I also thank the National Park Service, especially Kathy Mellander, for technical support.

Literature Cited

Arsenault, A.M. and A.J. Meigs, 2005.Contribution of deep-seated bedrock landslides to erosion of a glaciated basin in southern Alaska. Earth Surface Processes and Landforms, 30: 1111-1125.

Bradley, F. H., 1873. Geological report of the Snake River Division. In: 6th Annual report of the U, S. Geological Survey of the Territories; 191-271.

Byrd, J.O.D., R.B. Smith, J.W. Geissman, 1994. The Teton Fault, Wyoming: Topographic signature, neotectonic, and mechanisms of deformation. Journal of Geophysical research: Solid Earth; 99 (B10): 20095 20122.

Case, J.C., 1989. Wyoming landslide classification scheme. Geologic Hazards Section, Wyoming State Geological Survey (www.wrds.uwyo.edu).

Cossart, E.; Braucher, R.; Fort, M.; Bourlès, D.L.; Carcaillet, J., 2008. Slope instability in relation

to glacial debuttressing in alpine areas (Upper Durance catchment, southeastern France): Evidence from field data and ^{10}Be cosmic ray exposure ages. Geomorphology, 95, (1-2) :3-26.

Foster, D., S.H. Brocklehurst, R.L. Gawthorpe, 2010. Glacial-topographic interactions in the Teton Range, Wyoming. Journal of Geophysical Research 115:

Edmunds, J., G. Kerr, S. Ramesh, and L. Pochop, 2011. Glacier variability (1967-2006) in the Teton Range, Wyoming, United States. Journal of the American Water Resources Association (JAWRA): 1-10.

Foster, D., S.H. Brocklehurst, R.L. Gawthorpe, 2010. Glacial-topographic interactions in the Teton Range, Wyoming. Journal of Geophysical Research 115:

Fryxell, F.M., 1930. Glacial features of Jackson Hole, Wyoming. Augustana Library Publications No. 13.

Fryxell, F., 1935. Glaciers of the Grand Teton National Park of Wyoming. The Journal of Geology, 43(4): 363-369.

Giardino, J.R., J.F. Shroder, Jr. and J.D. Vitek, (editors), 1987. Rock Glaciers. Allen & Unwin Co., London, UK, 355 p.

Hampel, A., R. Hetzel, A.L. Densmore, 2007. Post glacial slip-rate increase on the Teton normal fault, northern Basin and Range Province, caused by melting of the Yellowstone ice cap and deglaciation of the Teton Range? Geology, 35 (12): 1107 1110.

Hewitt, K., 2006. Disturbance regime landscapes: mountain drainage systems interrupted by large rockslides. Progress in Physical Geography 30(3): 365-393.

Licciardi, J.M. and Pierce, K.L., 2008. Cosmogenic exposure-age chronologies of Pinedale and Bull Lake glaciations in greater Yellowstone and the Teton Range, USA. Quaternary Science Reviews, 27(7-8): 814-831.

Love, J.B., J.C. Reed, K.L. Pierce, 2003. Creation of the Teton Landscape. Grand Teton Natural History Association, WY. 132 p.

Love, J.D., J.C. Reed, and A.C. Christiansen, 1992. Geologic Map of Grand Teton National Park. U.S. Geological Survey Miscellaneous Investigations Series Map I 2031, scale 1:62,500.

Love, J.D., J.C. Reed, Jr., and K.L. Pierce, 2007. Creation of the Teton landscape: A Geological Chronicle of Jackson Hole and the Teton Range2nd ed., Salt Lake City (UT): Paragon Press.

Marston, R.A., B.J. Weihs, W.D. Butler, 2011. Slope failures and cross-valley profiles, Grand Teton National Park, Wyoming. In: National Park Service Research Center; 33rd Annual report 2011. (eds.) H.J. Harlow and M.A. Harlow; University of Wyoming; 51- 64.

Pierce, KL, Good, JD, 1992. Field Guide to the Quaternary geology of Jackson Hole, Wyoming. U.S. Geological Survey Open File Report 92-504.

Pierce, K.L., 2003. Pleistocene glaciations of the Rocky Mountains. Development in Quaternary Science, 1; 63-76.

Reed, J.C., 1964. Recent retreat of the Teton Glacier, Grand Teton national Park, Wyoming. U.S. Geological Survey Professional Papers, 501C: C147-C151.

Reed, J.C., 1967. Observations of the Teton Glacier, Grand Teton National Park, Wyoming, 1965 and 1966. U.S. Geological Survey Professional Papers 575C: C154-C159.

Shroder, J.F., Jr., and Sewell, R.E., 1985. Mass Movement in the La Sal Mountains. In Christenson, G.E., Oviatt, C.G., Shroder, J.F., Jr., Sewell, R.E. (eds), Contributions to Quaternary Geology of the Colorado Plateau. Utah Geological and Mineral Survey Special

Studies, 64, 48-85.

Shroder, J.F., Jr., 1998a. Slope failure and denudation in the western Himalaya. Special volume on “Mass Movement in the Himalaya”; ed. J.F. Shroder, Jr.; Geomorphology, 26: 81-105.

Shroder, J.F., Jr., 1998b. Mass movement in the Himalaya: An Introduction. Special volume on “Mass Movement in the Himalaya”; ed. J.F. Shroder, Jr.; Geomorphology, 26: 911.

Shroder, J.F., Jr., 1998c. Mass movement in the Himalaya: An Introduction. Special volume on “Mass Movement in the Himalaya”; ed. J.F. Shroder, Jr.; Geomorphology, 26: 9 11.

Shroder, J.F., Jr. and M.P. Bishop, 1998. Mass movement in the Himalaya: new insights and research directions. Special volume on “Mass Movement in the Himalaya”; ed. J.F. Shroder, Jr.; Geomorphology, 26: 13-35.

Shroder, J.F., Jr., R. A. Scheppy, and M.P. Bishop, 1999. Denudation of small alpine basins, Nanga Parbat Himalaya, Pakistan. Arctic, Antarctic, and Alpine Research, 31: 99-105.

Shroder, J.F., Jr., L. Čverčkova, K. Mulhern, 2005. Slope-failure analysis and classification: Review of a century of effort. Physical Geography, 26 (3): 216-247.

Shroder, J.F.,Jr., L.A. Owen, Y.B. Seong, M.P. Bishop, A. Bush, M.W. Caffee, L. Copland, R.C. Finkel, U. Kamp, 2010. The role of mass movements on landscape evolution in the Central Karakoram: Discussion and speculation. Quaternary International, doi:10.1016/j.quaint.2010.05.024.

Shroder, J.F., Jr., B. Weihs, and M. Schettler, 2011. Mass movement in northeast Afghanistan. Journal of Physics and Chemistry of the Earth; 36:1267-1286; doi:10.1016/j.pce.2011.03.003.

Shroder, J.F., Jr. and B.J. Weihs, 2010. Geomorphology of the Lake Shewa landslide dam,

Badakshan, Afghanistan, using remote sensing data. Geografiska Annaler 92A (4):471-486.

Smith, R.B., J.O.D. Byrd, D.D. Susong, 1993. The Teton Fault, Wyoming: seismotectonics, Quaternary history, and earthquake hazards. In: Snoke, A.W., J.R. Steitdmann, and S.M. Roberts, editors, Geology of Wyoming: Geological Survey of Wyoming Memoir No. 5: 628-667.

St. John, O., 1879. Geological Report of the Teton Division. In: 11th Annual Report of the U.S. Geological Survey of the Territories; 321-508.

Stoffel, M. and C. Huggel, 2012. Effects of climate change on mass movements in mountain environments. Progress in Physical Geography; 36(3): 421-439.

Tranel, L.M., J.A. Spotila. M.J. Kowalewski, C.M. Waller, 2011. Spatial variation of erosion in a small, glaciated basin in the Teton Range, Wyoming, based on detrital apatite (U –Th)/He thermochronology. Basin Research 23: 5711-590.

Figures and Figure Captions

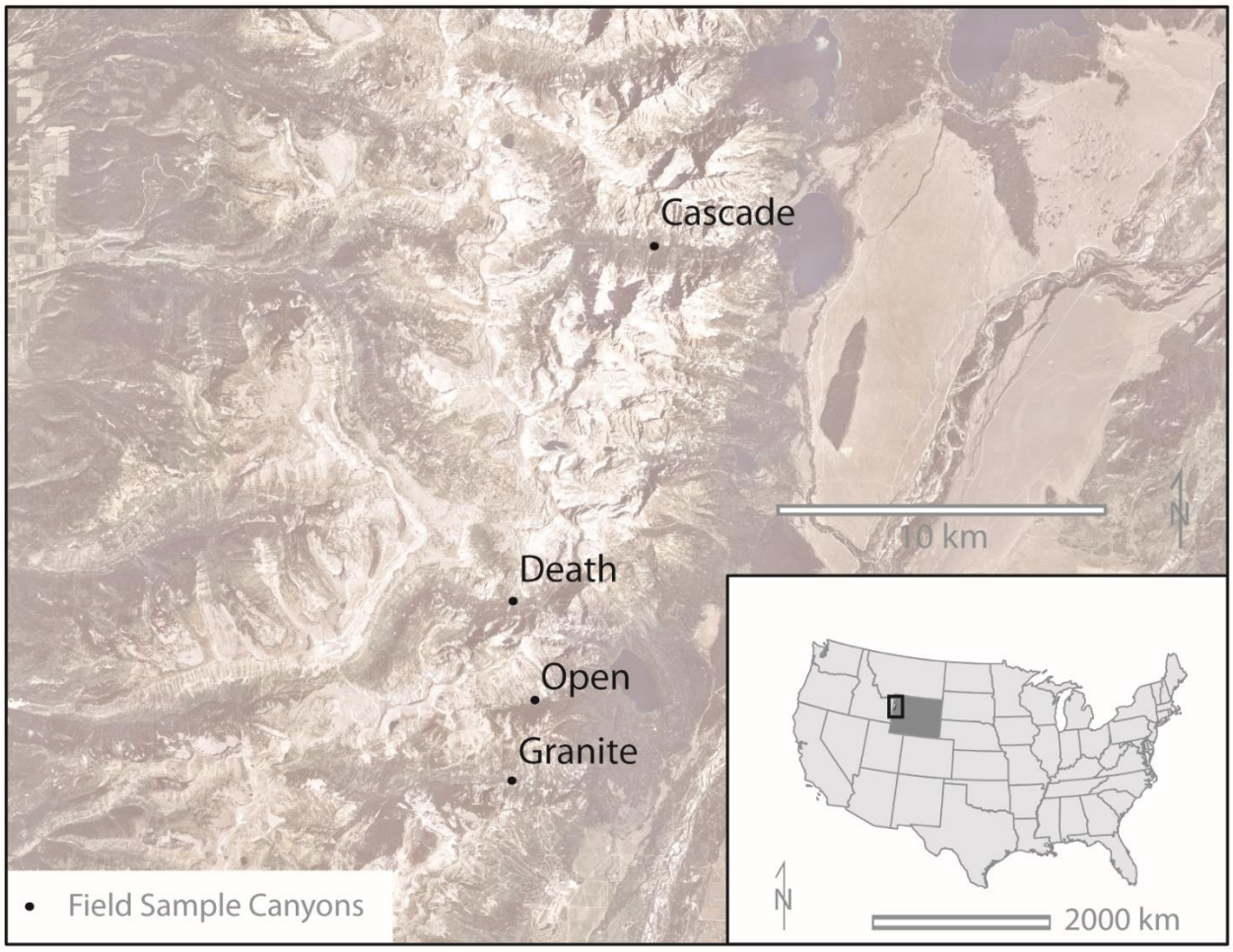

Figure 3.1. Study area canyons of Grand Teton National Park.

Figure 3.2. Planimetric view of opposing debris flow deposits and subsequent impoundment in Cascade Canyon using NAIP aerial photo (2009).

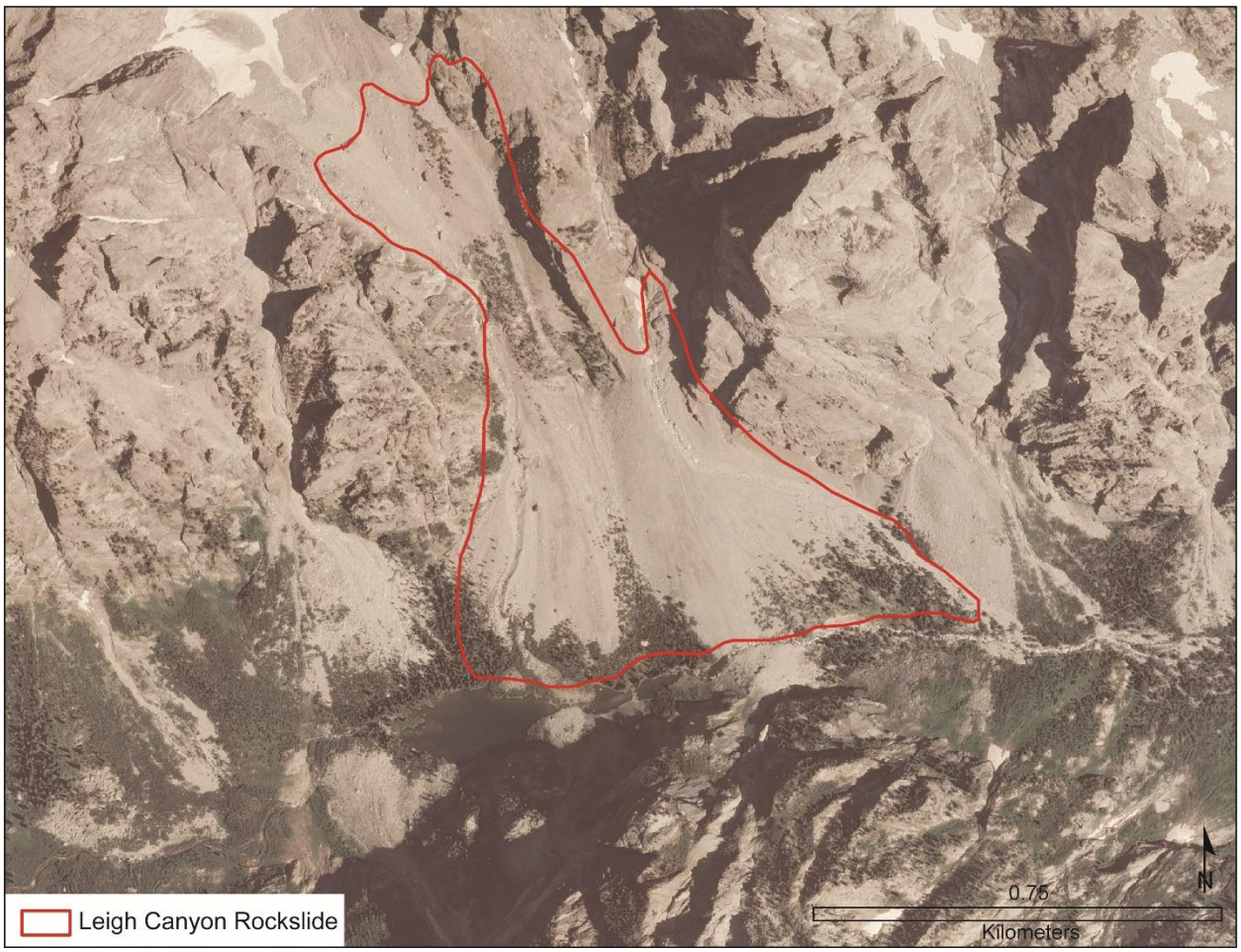

Figure 3.3. Planimetric view of a rockslide deposit and subsequent impoundment in Leigh Canyon using NAIP aerial photo (2009).

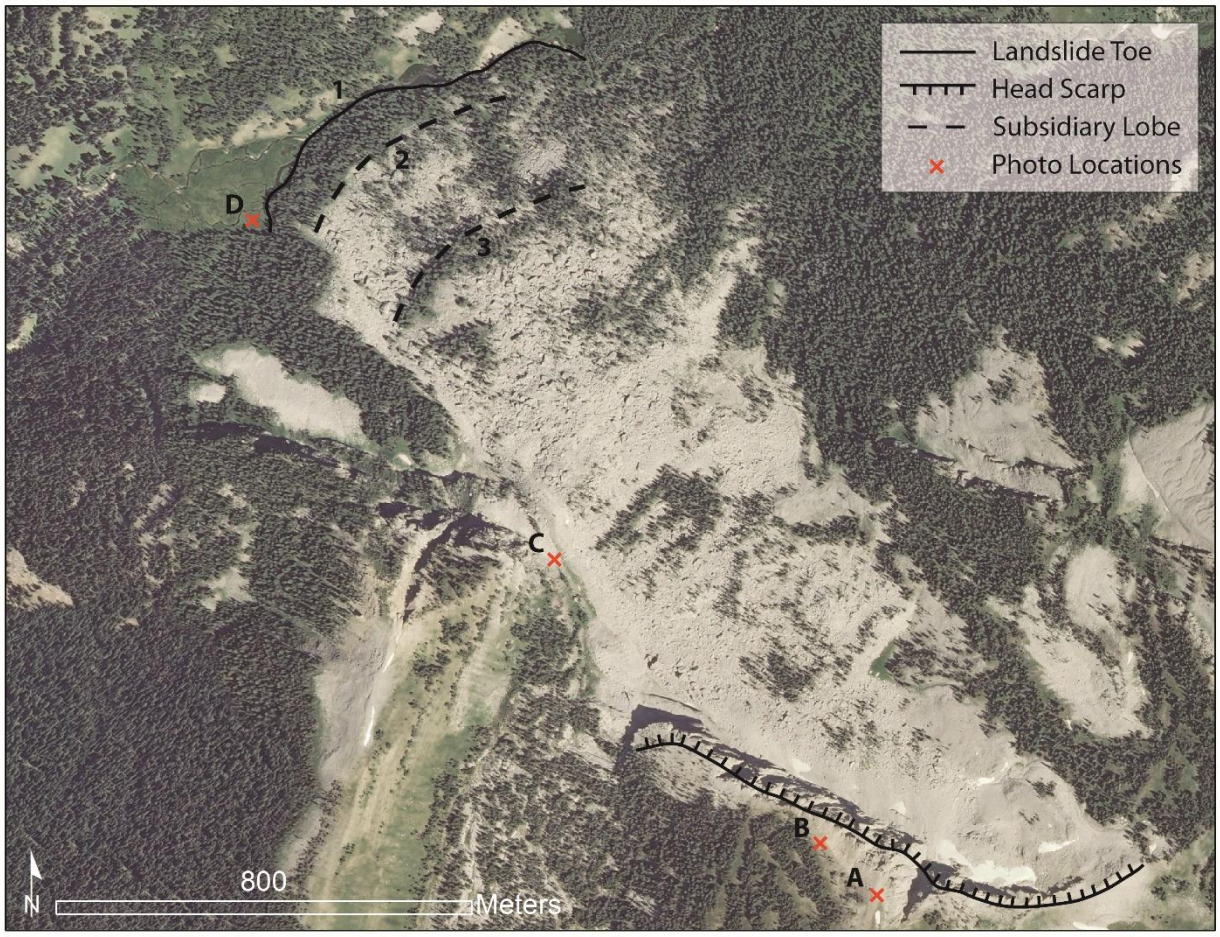

Figure 3.4. Planimetric view of Rendezvous Rockslide using NAIP aerial photo (2009). Adjacent photos are located on map with red X's. Several lobes (1, 2, 3) are thought to represent at least three separate failure events contributing to this deposit.

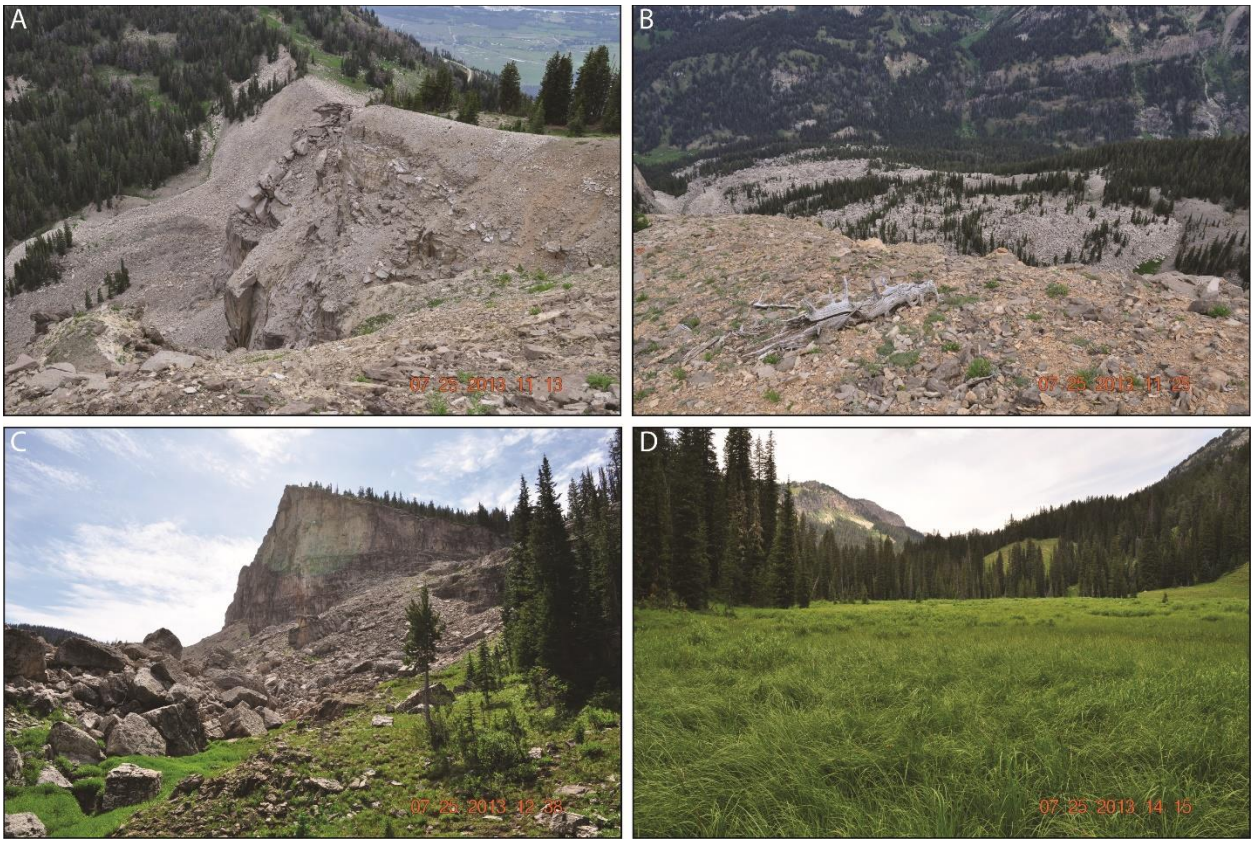

Figure 3.5. Photos taken at Rendezvous Rockslide. Photos A & B taken at head scarp. Photo C was taken at mid-slope and margin of landslide. Photo D was taken at the landslide toe, which caused impoundment of Granite Creek and the deposition of sediments in this now-drained lake.

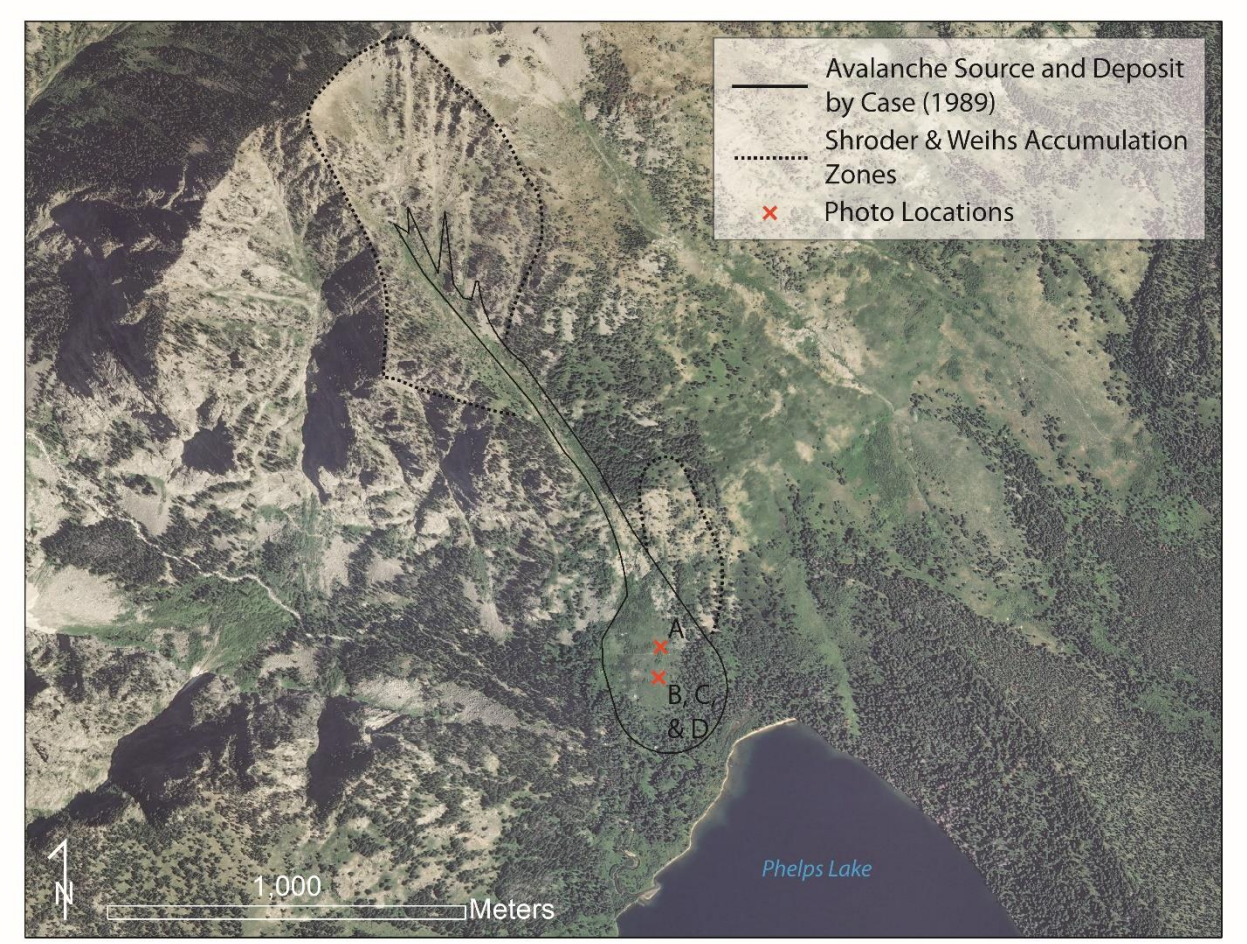

Figure 3.6. Planimetric view of Death Canyon avalanche source and deposit using NAIP aerial photo (2009). Avalanche polygon delineated by Case (1989) (solid line) was modified in this study (dashed line). Adjacent photos are located on map with red X's.

Figure 3.7. Photos taken in and near Death Canyon of an avalanche source and deposit. Figure A shows source area. Figure B shows large boulder transported during 2010-2011 avalanche season. Figures C & D show still growing downed trees beneath boulder and on deposit.

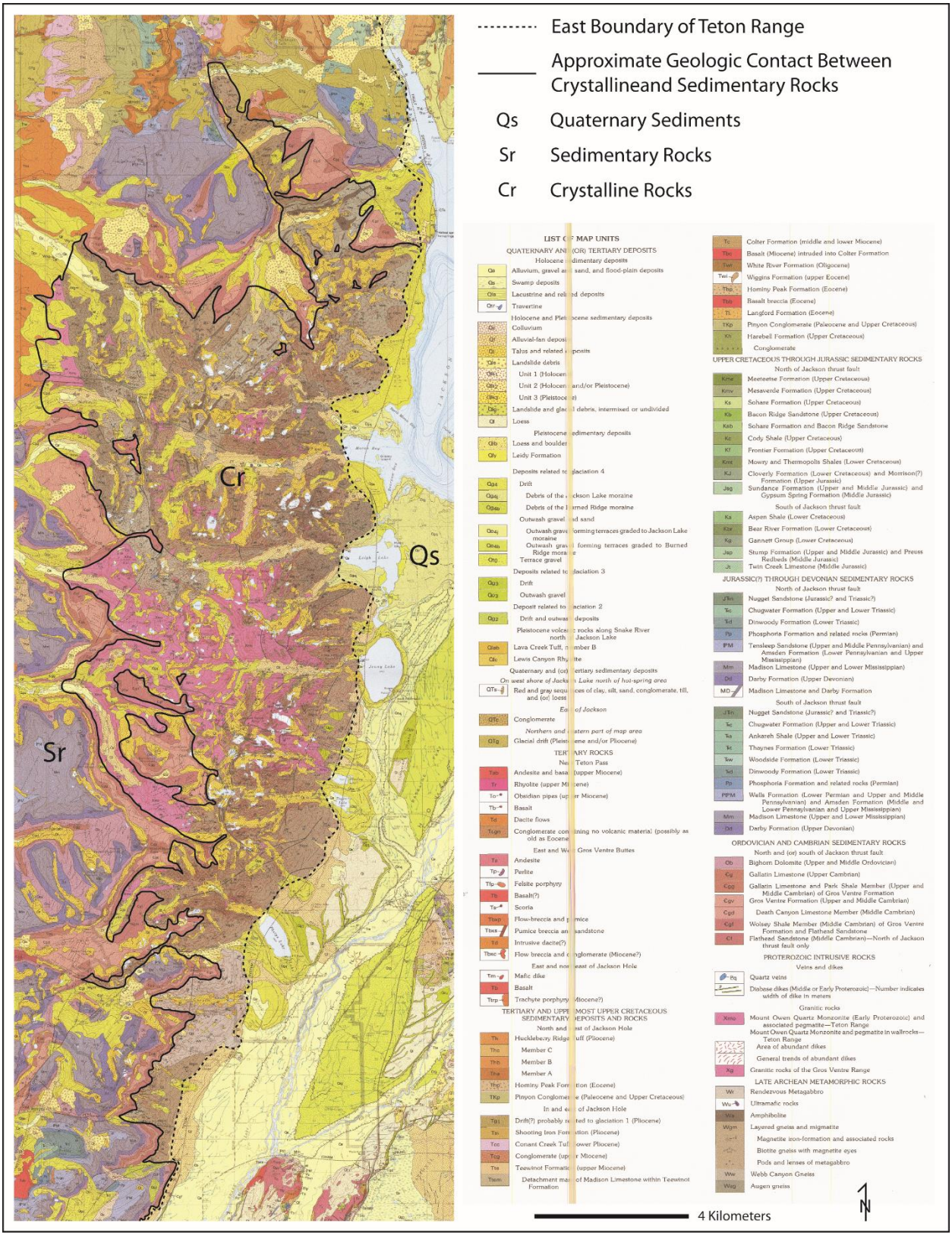

Figure 3.8. Geologic map of the Teton Range. Modified from Love et al. (1992).

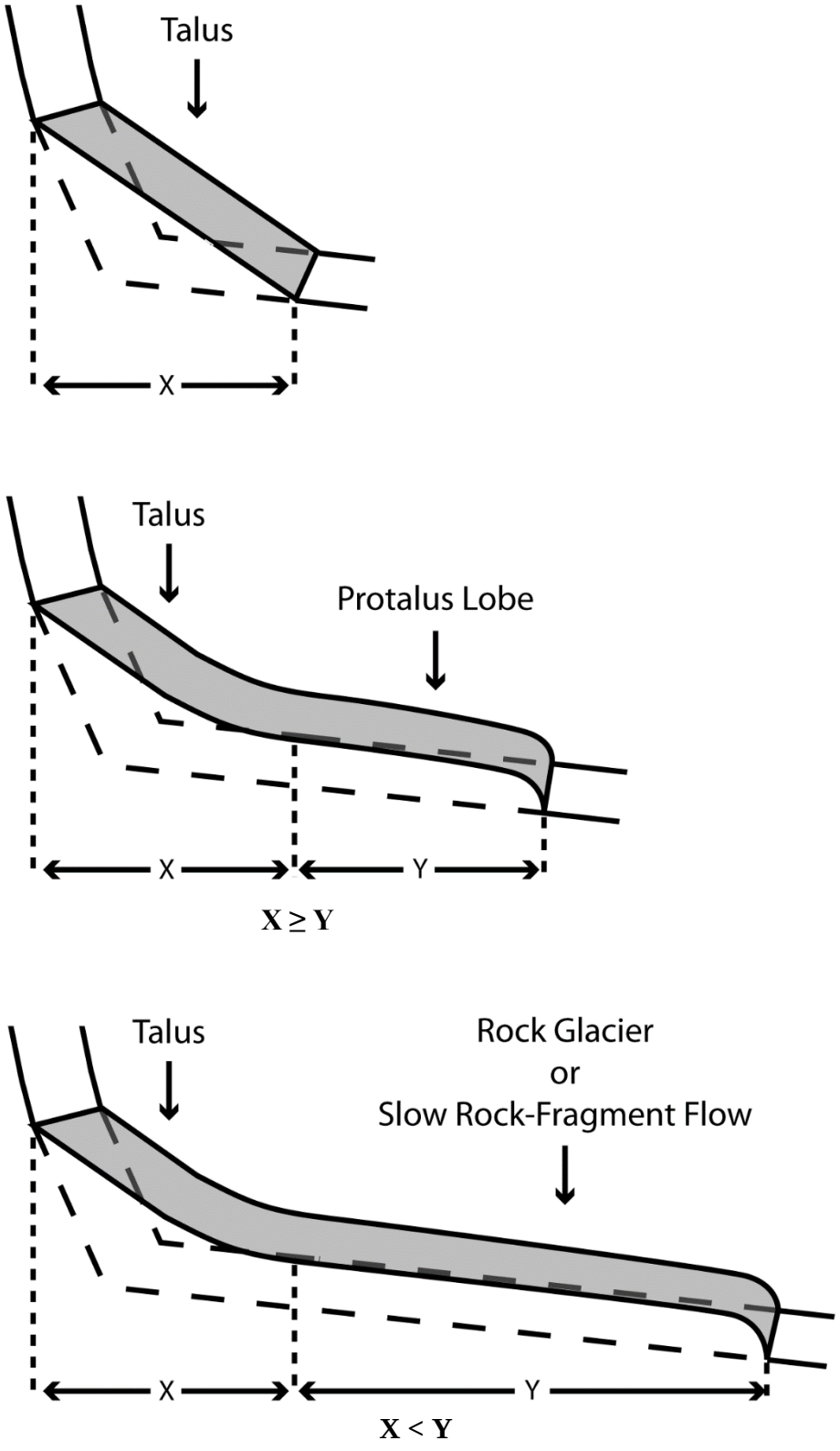

Figure 3.9. Generalized graphic of talus slopes, protalus lobes, and rock glaciers or slow rock-fragment flows. Modified from Shroder and Sewell (1985).

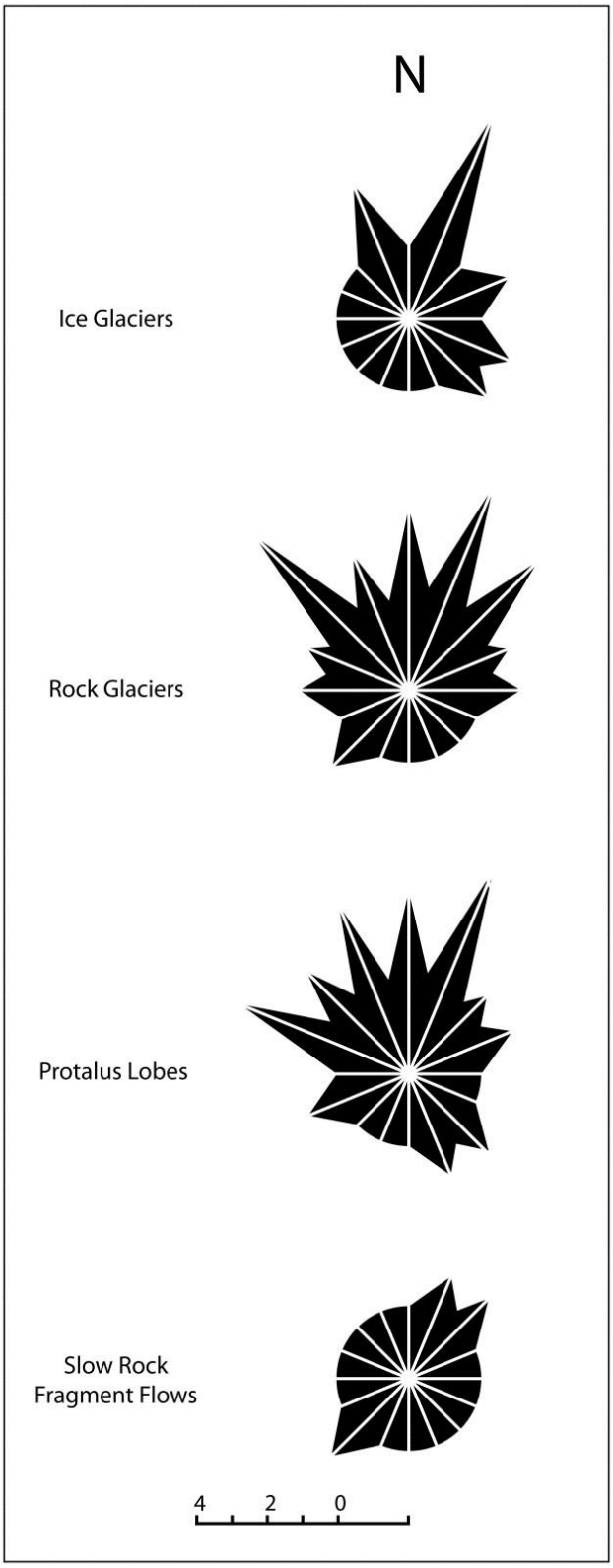

Figure 3.10. Radar diagrams of aspect directions of various deposits in GTNP. Note that these data represent features mapped for this project, and not for the entirety of the range.